

# TORQUE ESTIMATION OF DOUBLE FED INDUCTION GENERATOR USING A DYNAMIC MODEL AND MEASURED DATA

Master Thesis  
November 2010



---

**Kristofer Nilsson**

Dept. of Industrial Electrical Engineering and Automation  
Lund University



# TORQUE ESTIMATION OF DOUBLE FED INDUCTION GENERATOR USING A DYNAMIC MODEL AND MEASURED DATA

<b>From</b> Vattenfall Research and Development AB, UPV	<b>Date</b> 2010-05-09	<b>Serial No.</b>
<b>Author/s</b> Kristofer Nilsson	<b>Access</b> Full Access	<b>Project No.</b> PR.138.1.103.32
<b>Customer</b>	<b>Reviewed by</b>	
	<b>Issuing authorized by</b>	
<b>Key Word</b>	<b>No. of pages</b> 52	<b>Appending pages</b> 10

## Summary

A big challenge in the Wind Power industry is the breakdown of gearboxes. To increase the knowledge about Wind Power and gearbox breakdowns Vattenfall has done measurements on both the mechanical and electrical system of a wind power turbine e.g. during full load and partial load. In this Master Thesis focus is on voltage and current measurements on the generator conductors and the measurements of the rotor speed. Different run scenarios for a wind power turbine have been studied and analysed briefly. Secondly a mathematical model in MATLAB/Simulink has been built, which calculates a corresponding mechanical torque based on the electrical measurements. To further improve the results from the model, more accurate speed measurements have to be done. For future work it would be interesting to compare the results from an improved model with mechanical measurements.

## Abstract

A big challenge in the Wind Power industry is the breakdown of gearboxes. To increase the knowledge about Wind Power and gearbox breakdowns Vattenfall has done measurements on both the mechanical and electrical system of a wind power turbine e.g. during full load and partial load. In this Master Thesis focus is on voltage and current measurements on the generator conductors and the measurements of the rotor speed. Different run scenarios for a wind power turbine have been studied and analysed briefly. Secondly a mathematical model in MATLAB/Simulink has been built, which calculates a corresponding mechanical torque based on the electrical measurements. To further improve the results from the model, more accurate speed measurements have to be done. For future work it would be interesting to compare the results from an improved model with mechanical measurements.

# Table of Contents

Page

<b>1</b>	<b>INTRODUCTION</b>	<b>3</b>
1.1	Background	3
1.2	Problem Definition	3
	1.2.1 Purpose	3
	1.2.2 Goal	3
<b>2</b>	<b>DRIVE TRAIN RELIABILITY</b>	<b>5</b>
2.1	Gearbox	5
2.2	Gearbox Failure	6
2.3	Aspects of Gearbox Failure	7
<b>3</b>	<b>THEORY</b>	<b>8</b>
3.1	The Wind	8
3.2	Double Feed Induction Generator and Power Electronics	8
3.3	Control of Wind Turbines	10
3.4	Mathematical Modelling of Double Feed Induction Generator	11
	3.4.1 Electrical dynamics	11
	3.4.2 Mechanical dynamics	15
3.5	Converter	15
	3.5.1 Pulse width modulated converter	15
<b>4</b>	<b>OPERATIONAL SITUATIONS</b>	<b>19</b>
4.1	Normal Production	19
4.2	Curtailed	19
4.3	Normal Stop	19
4.4	Emergency Stop	19
4.5	Star/ $\Delta$ Switch	20
4.6	Over Speed	21
4.7	Start Up	21
4.8	Idling	21
<b>5</b>	<b>METHOD</b>	<b>22</b>
5.1	Measurement Setup	22
	5.1.1 Test turbine	22
	5.1.2 Electrical setup	22
	5.1.3 Mechanical setup	23
	5.1.4 Measurement limitation	23

5.2	Data Processing	24
5.2.1	Stator angle	24
5.2.2	Rotor angle	25
5.2.3	Velocity and acceleration	26
5.3	Model	27
5.3.1	Parameters	27
5.4	Simulation Signals	28
5.4.1	Stator current	28
5.4.2	Rotor current	29
5.4.3	Angle, velocity and acceleration	31
<b>6</b>	<b>ANALYSIS AND RESULTS</b>	<b>34</b>
6.1	Electrical Measurements	34
6.2	Simulations	36
6.2.1	Verifying the model	36
6.2.2	Uncertainties	37
6.2.3	Curtailed run scenario with power reference 160 kW	38
6.2.4	Star/ $\Delta$ switch	39
<b>7</b>	<b>CONCLUSION</b>	<b>40</b>
<b>8</b>	<b>FUTURE WORK</b>	<b>41</b>
	<b>APPENDIX A</b>	<b>42</b>
	Simulation Block Diagrams	42
	<b>APPENDIX B</b>	<b>48</b>
	Simulation File	48
	<b>BIBLIOGRAPHY</b>	<b>52</b>

# Nomenclature

## Symbols

$P_{kin}$	Kinetic energy
$\dot{m}$	transported mass
$\rho$	air density
$A$	Sweep area
$\omega_e$	electrical rotor speed
$\omega_m$	mechanical rotor speed
$\omega_s$	synchronous speed
$p$	number of pole pairs
$\theta_{pitch}$	Pitch angle
$U_{dc}$	DC-link capacitor voltage
$P$	power
$Q$	reactive power
$v$	voltage
$i$	current
$\varphi$	magnetic flux
$R$	resistance
$B$	magnetic field
$\mu_0$	permeability constant
$L$	inductances
$\theta$	angular displacement from $\alpha/\beta$ -frame
$T_{dq}$	Park's transformation matrix
$\beta_s$	angle between stator d/q reference frame and "a" circuit
$u$	output voltage from converter
$e$	phase voltage
$u_z$	zero sequence signal
$\hat{u}$	voltage amplitude
$k$	linear gradient
$T$	torque
$J$	inertia
$H$	inertia constant of the shaft and generator in seconds
$S$	rated power
$l$	length of conductor'
$F$	Force
$h$	hours
$w$	slope of Wöhler line

## Subscripts

s	stator
r	rotor
a,b,c	conductor phase
mag	magnetising
g	generated
loss	lost
t	transferred
n	rated
e	electrical
m	mechanical
eq	equivalent
B	beraing

## Abbreviations

PWM	pulse width modulated
DFIG	double fed induction generator
HSS	high speed shaft
LSS	low speed shaft
SCADA	Supervisory Control And Data Acquisition



# 1 Introduction

## 1.1 Background

The Master Thesis “Torque Estimation of Double Fed Induction Generator using a Dynamic Model and Measured Data“ is done within Vattenfall Wind Research and Development program. Vattenfall wind R&D is a project co-financed by the Pan-European business unit wind and the group function strategies. The project is to support Vattenfalls expansion of wind power.

The wind power industry is growing. 2% of the world’s power production is wind energy and according to the “Global Wind Energy Council” wind power could meet 12% of the global power demand by 2020.

With the expansion of wind power the industry requests bigger wind turbines. The turbine size has gone from 500 kW turbines in 1990 to 5 MW turbines today. Turbines with gearboxes still have the same composition for the gearboxes as in 1990. The wind power industry has since the start experienced problems with gearbox breakdowns and the breakdowns seem to increase proportionally with the increase in turbine size. Experiments are carried out all over the world to figure out the root cause and solve it but still no solution is found.

## 1.2 Problem Definition

The Wind R&D program has performed measurements on the drive train and the conductors on a 2MW ocean based wind power turbine. The drive train on a wind power turbine is defined as the shafts and the gearbox. The measurements are done for different run scenarios a wind power turbine can be exposed to. The measurements are unique as test rig experiments because they are done during real conditions to investigate if the turbine is exposed to any unexpected loads during normal conditions. The measured data on the drive train are analysed by engineers at Vattenfall Research and Development [1]. The electrical measurements on the conductors has not been analysed and no joined analyse between the electrical and mechanical measurements has been done.

### 1.2.1 Purpose

For Vattenfall Research and Development a big challenge is to solve the problems with gearbox breakdowns in wind power turbines.

Different run scenarios or control strategies for the turbine could be the reason why gearboxes break. Analysing the electrical data could lead to new knowledge about gearbox breakdown. The purpose with this thesis is to work out a method which makes it possible to study how the generator affects the gearbox for different run scenarios.

### 1.2.2 Goal

The main goal with the Master Thesis is to build a general model of a wind power induction generator. A dynamic model that calculates the mechanical torque the wind has to produce to deliver the power measured in the conductors. Using the model it should be possible to

analyse how different run scenarios affect the mechanical torque and compare the electrical measurements with the mechanical.

No analyse has been done on the electrical measurements. Therefore one of the goals with this thesis is to do a first analyse of those measurements i.e. sort it after different operational situations and search for unexpected situations.

Currently the measurements on the drive train and the electrical conductors are done at different occasions. A third goal for this Master Thesis is to analyse the data from the power turbine and decide the benefits in redoing the measurement for the drive train and conductors at the same time.

## 2 Drive Train Reliability

Today most wind power turbines are equipped with a gearbox and an asynchronous generator. There are also turbines with synchronous generators that are equipped both with and without gearboxes.

The shaft connected to the turbine blades of the wind power turbine is called low speed shaft. The low speed shafts frequency is approximately 0.25-0.5 Hz. For an asynchronous generator the speed of the high speed shaft, the shaft connected to the generator's rotor, must be slightly above 25 Hz for optimal production. The so called double feed induction generator (DFIG) that is more described in Chapter (3.2) can compensate for speed variations up to 30%. This means the speed must be geared up approximately 100 times for a four pole DFIG. The alternatives to DFIG with gearbox is synchronous or induction generator with converters that rectifies all current and then transfers it back to alternating current, through a full power converter. This is done for synchronous generator both with and without gearboxes [3]. Until today this solution has been secondary to the DFIG due to high losses in the converters and a large generator size required. But as the losses and cost decreases with the development of the converters it becomes more common to use full power converters instead of gearboxes.

### 2.1 Gearbox

The wind power gearbox increases the speed of the shaft between the hub and the generator. The low speed shaft is supported by two main bearings, one fix and one floating. The gearbox is connected to the low speed shaft via shrink disc element, to the generator via composite coupling and to the nacelle via elastic support. A hydraulic oil conditioning system is used for lubrication. The gearbox in the test turbine is built up of one planet gear and two helical gears as shown in Figure 1 [16]. The planet gear has three planet gearwheels rotating around the sun wheel. Together with the helical gears this gives a gear ratio of 92:1 [5].

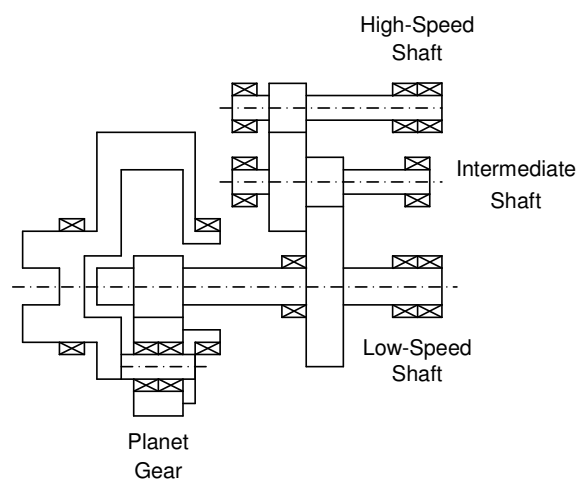


Figure 1: Wind Power Gearbox for a general 2 MW turbine

A wind turbine has a designed lifetime of 20 years. That corresponds approximately to 120.000 hours production. For the gearbox to withstand the forces and wear a robust design is needed [15].

When dimension the bearings in the gearbox the calculations are based on the load equivalent  $T_{eq,B}$  [13]. The equivalent is calculated according to:

$$T_{eq-B} = \left( \frac{h_1 T_1^w + \dots + h_{n+1} T_{n+1}^w}{\sum h_n} \right)^{\frac{1}{w}} \quad (1)$$

where  $T$  is the torque level for a monitored interval  $T_{n-1} < T < T_{n+1}$  and  $h$  is the duration in hours for the same interval.  $w$  is the slope of the Wöhler line. The Wöhler line is a plot between the cyclic stress and the logarithmic scale of the number of samples until failure [14]. In the method to calculating the equivalent torque the speed and the oil temperature are assumed to be constant. The equivalent load is in the range of 65-75% of the nominal load [13].

## 2.2 Gearbox Failure

Two of Vattenfalls wind power farms are operating Vestas V80 and V90, power turbines that are equipped with gearboxes and asynchronous generators. They are located at Horns Rev in Denmark that was taken into operation during 2002 and Thanet in Great Britain that has been commissioned in 2010. At Horns Rev 80 offshore Vestas V80-2 MW turbines are in operation and in Thanet - that is one of the world's largest offshore Wind Power farms- have 100 offshore Vestas V90-3 MW turbines. Both Vestas V80 and V90 have DFIG generators and gearboxes.

At Horns Rev 80-85% of all gearbox failures it is either the planet bearing or the high speed shaft bearing that breaks down, the bearing can be seen in Figure 2. Only in 1 or 2% of the failures the cause is known [13]. If a high speed shaft bearing breaks it can be changed on location. If a planet bearing breaks the whole gearbox must be changed. The planet bearing is then changed in a workshop. The repair of the bearings is a very costly procedure. This is not only due to costs for components and maintenance personnel, but also because the wind power turbine can not produce any energy during the breakdown hence a loss of income for the power company. For Horns Rev the breakdown of the planetary bearings started already in the first year after commissioning. No root cause has been concluded, therefore many different aspects of the problem are analysed.

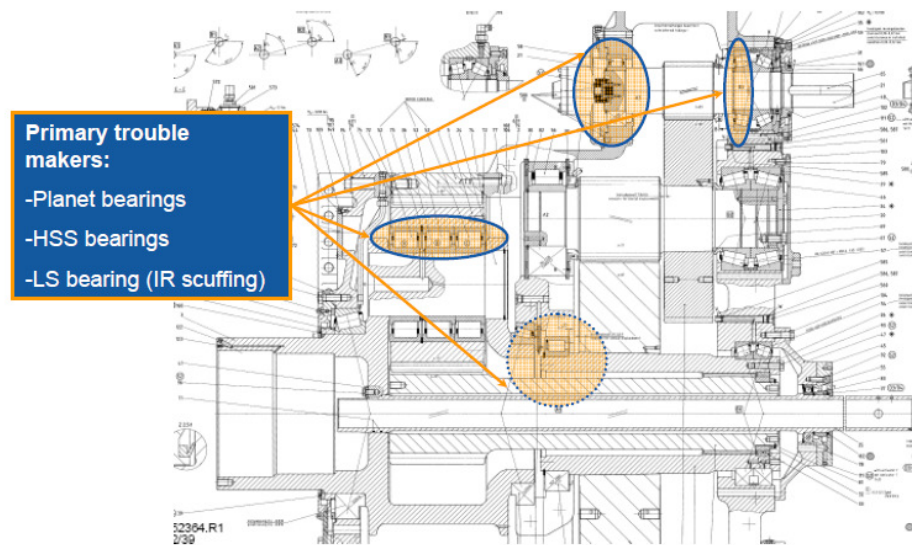


Figure 2: Gearbox drawing with bearings highlighted.

### 2.3 Aspects of Gearbox Failure

Analysis done on the bearings from broken gearboxes shows that the most frequent cause for failure is overload [13]. One of the run scenarios that cause high forces on the turbine and its gearbox that could lead to overload is emergency stop, when the turbine stops in the duration of a couple of seconds. This case has been studied and no relation between emergency stop and gearbox failure has been concluded.

The breakdowns are statistical consistent. This could indicate that the gearbox is designed or manufactured with poor quality or inadequately strength and robustness. The gearbox quality level has been researched and verified and according to calculations the design is sufficient. The calculations and verifications for the gearbox design are for an estimated environment. The turbine on which the measurements are done is stipulated for wind speeds of 8.5 m/s and the mean wind is 9.5-10 m/s. This should only lead to reduced fatigue life time with 30-35%. One of the main reasons for the measurements is that the turbine could impose unexpected load scenarios trough transient. Transient generated electrical or by external regulations. Transient generated electrical could be low voltage ride through, grid-off or faults leading to low torque or over speed situations, all cases that could creating reversal torque. Different pitch and converter algorithms could also lead to low torque. External regulation that controls the output power of the wind turbine to a certain set level could lead inadequate traction forces in the bearing elements. Vestas how is the manufacturer of the turbine has change the minimum set level from 160 kW to 200 kW.

This indicates that the root cause for the breakdowns is incredible difficult to define. The design is verified, the gearbox is tested for overload in test rigs and the gearboxes are monitored with Condition Monitoring Systems and still the cause for the breakdowns are unknown. The gearboxes seems to be imposed to load not handled by the design methodology. This could be high loads, low loads or varying loads not taken in consideration during the design. The problem is to define “the killer”, the cause for the breakdowns.

## 3 Theory

This thesis is aimed towards wind power turbines with double feed induction generator. All the theory in this section is for a general double feed induction engine.

### 3.1 The Wind

The energy the wind contains can be transferred to mechanical energy. The kinetic energy in the wind can be expressed as:

$$P_{kin} = \frac{1}{2} \dot{m} v^2 \quad (2)$$

$$\dot{m} = \rho A v \quad (3)$$

where  $\dot{m}$  is the mass transported,  $\rho$  the air density,  $A$  the sweep area of the rotor blades and  $v$  the speed of the wind [3]. If the area and the air density are approximated to be constant then the kinetic energy can be expressed as:

$$P_{kin} = \text{constant} \cdot v^3 \quad (4)$$

From Equation (4) it is concluded that the energy of the wind is proportional to the wind speed to the power of three. The power curve for a wind power turbine is unique for each turbine depending on unique losses in the turbines. The power curve for a 2 MW turbine can be seen in Figure 3 [5].

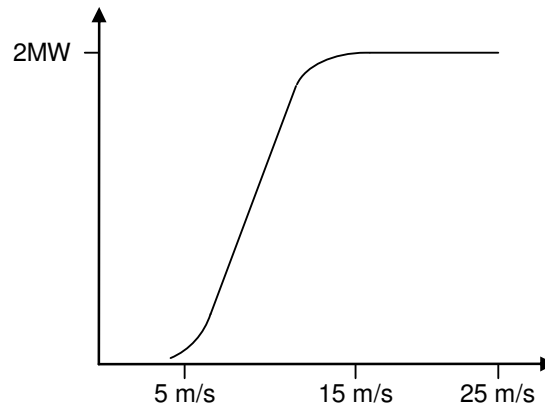


**Figure 3: Example of a power curve for a 2 MW turbine**

A wind power turbine is shut down if the wind speed is less than around 3 to 5 m/s. In lower wind speed the vibrations will be undesirably high because the electromagnetic torque is not high enough to level out small torque variations that can lead to fatigue. Above 25 m/s the forces from the wind on the power turbine becomes too high and the power turbine has to be stopped for safety reasons. Nonoperational power turbines can withstand wind speed up to 60 m/s. The efficiency for a generator is highest at full power production and is decreasing with decreasing wind speed. Because the generator often is run below full power the production can be optimised for lower wind speed by pitching the blades and controlling the generator, see Chapter (3.3).

### 3.2 Double Feed Induction Generator and Power Electronics

The principle for an induction engine and an induction generator are the same. So for the general understanding let us consider the induction engine with a squirrel cage rotor. The

squirrel cage rotor has slots with bars of aluminium or copper that is short circuit in the ends embedded in the structure. In Figure 4 the short circuited bars without the structure are shown.

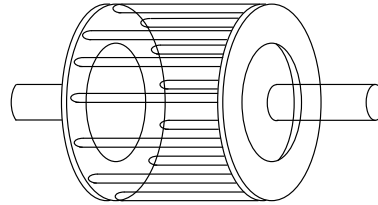


**Figure 4: Squirrel cage rotor**

If the stator is connected and magnetized from the grid the magnetic field in a three phase stator with one pole pair will rotate with the synchronous speed of 50 Hz. If friction and other losses are disregarded, the squirrel cage rotor will rotate with the synchronous speed in a no load situation. The engine is in equilibrium and will not produce any torque [4]. If a load is added, the rotor slows down below the synchronous speed and the magnetic field generated in the stator will pass the bars in the rotor and a current will be induced in the bars. The current goes through the bars and creates a magnetic field in the rotor.

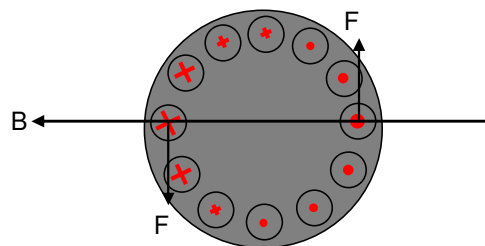


**Figure 5: Magnetic field B and Forces F on the squirrel cage rotor**

The rotor and stator creates one joint magnetic field B. This magnetic field and the current induced in the rotor produce the force F according to:

$$F = Bil \quad (5)$$

where  $i$  is the current in the conductor and  $l$  is the length of the conductor. The forces  $F$  create the mechanic torque. The induction generator always tries to reach equilibrium. If the generator rotates with the synchronous speed and a torque is added that accelerate the rotor speed above the synchronous speed the engine becomes a generator instead. In the double feed induction generator (DFIG) the squirrel cage rotor is replaced with a wound rotor. A wound rotor is built up the same way as a stator with three-phase winding distributed symmetrically around the rotor as shown in Figure 9. The number of pole pairs in the generator decides the electrical synchronous speed according to:

$$\omega_e = p\omega_m \quad (6)$$

where  $p$  is the number of pole pairs and  $\omega_m$  is the mechanical speed of the rotor. The rotor is connected to a back-to-back converter via a slip ring. The converter is in its turn connected to the power grid as shown in Figure 6, allowing approximately 30% of the generator power to be transferred via the rotor.

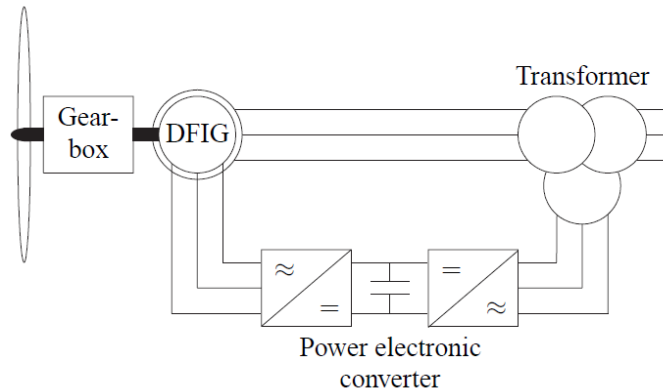


**Figure 6: Double feed induction generator with power converter**

By controlling the rotor current via the converter it is possible to have a varying rotor speed and still a synchronous output to the power grid from the stator. In super synchronous speed the DFIG is in generator mode and produce power both in stator and rotor. When in sub synchronous speed power must be added through the rotor via the converter to be able to stay in generator mode and produce power in the stator windings. The ability to control the current in the rotor also makes it possible to compensate for the reactive power needed to magnetize the generator and for some reactive power in the power grid.

### 3.3 Control of Wind Turbines

The main goal for the wind turbine controller is to maximize the output from the system. An overview of a general control system for a double fed induction generator is shown in Figure 7.

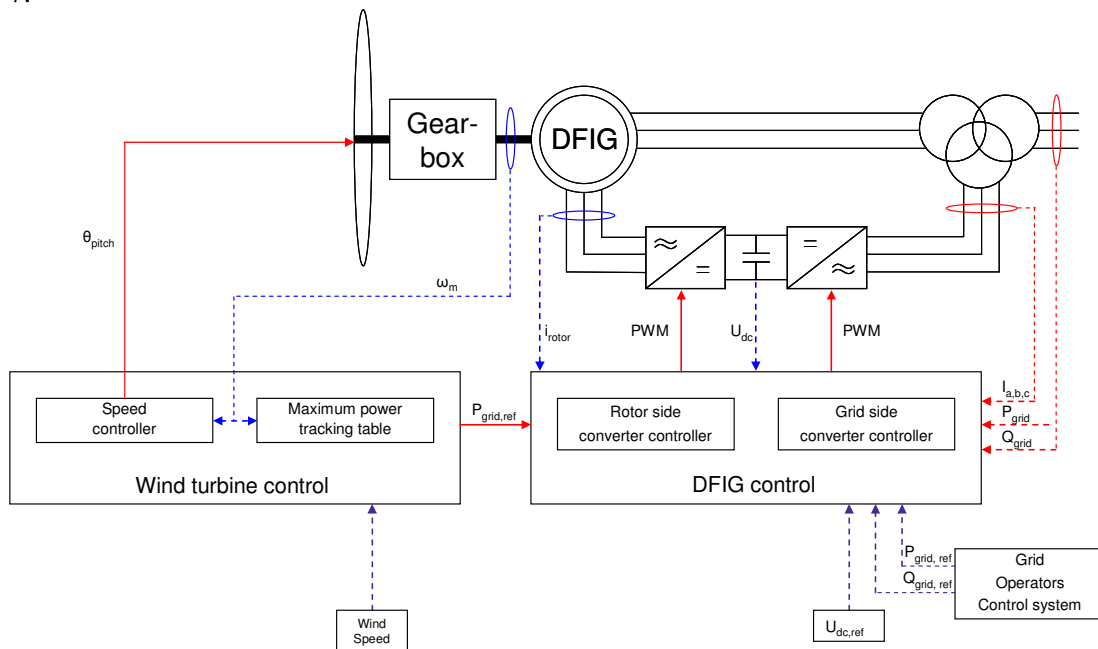


**Figure 7: Control system of Wind Turbine**

The “DFIG controller” that is a fast dynamic loop controls the rotor and grid side converters. The rotor side converter controls the current to the rotor. The grid side converter controls the



DC link voltage,  $U_{dc}$  and the power flow between the rotor and the power grid to be pure active power [6]. The “wind turbine controller” that has a much slower dynamic control loop than the “DFIG controller”, provides both the pitch system and the “DFIG controller” with reference values. The power reference,  $P_{grid,ref}$  to the “DFIG controller” seen in Figure 7 is based on a look up table. This reference is a optimal power and rotor speed calculated for low winds. For high wind speed the criteria is based on maximum rotor speed and noise level. The rotor speed is limited to  $\omega_{max}$  by the speed controller that controls the pitch angle  $\theta_{pitch}$ . The control system is built up hierarchically and grid operators can override the optimal power references and set the power production and reactive power production to a certain desired level.

### 3.4 Mathematical Modelling of Double Feed Induction Generator

Unless anything else is mentioned the dynamic equations used are based on [7]. It is used because it is a public report for a general double fed induction generator with the dynamics equations derived.

#### 3.4.1 Electrical dynamics

A conductor placed in motion in a magnetic flux gets a voltage induced according to Faraday’s law

$$v = \frac{d\varphi}{dt} \quad (7)$$

where  $v$  is the voltage and  $\varphi$  is the magnetic flux [8]. With equation (7) and known resistance in the coils and circuits in the stator and rotor it is possible with Kirchoff’s law to derive the voltage equations for an induction machine:

$$\begin{bmatrix} v_{as} \\ v_{bs} \\ v_{cs} \end{bmatrix} = R_s \begin{bmatrix} i_{as} \\ i_{bs} \\ i_{cs} \end{bmatrix} + \frac{d}{dt} \begin{bmatrix} \varphi_{as} \\ \varphi_{bs} \\ \varphi_{cs} \end{bmatrix} \quad (8)$$

$$\begin{bmatrix} v_{ar} \\ v_{br} \\ v_{cr} \end{bmatrix} = R_r \begin{bmatrix} i_{ar} \\ i_{br} \\ i_{cr} \end{bmatrix} + \frac{d}{dt} \begin{bmatrix} \varphi_{ar} \\ \varphi_{br} \\ \varphi_{cr} \end{bmatrix} \quad (9)$$

where the subscripts  $r$  and  $s$  denotes rotor and stator,  $a$ ,  $b$  and  $c$  denotes the different phases and  $R$  the resistance. The current are defined as going into the machine from the power grid. When a current runs through a coil it produces a magnetic field according to

$$B = \frac{\mu_o I}{2\pi r} \quad (10)$$

The magnetic field  $B$  is proportional to the current, inversely proportional to the distance with the permeability constant  $\mu_o$  [8]. The magnetic field will induced a voltage into the different bars in the rotor and build a magnetic field according to Figure 8 [9] for the squirrel cage rotor. The same principle goes for a wound rotor.

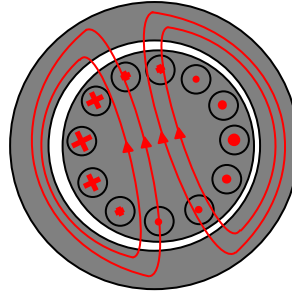


**Figure 8: Rotor flux**

If the magnetic field is integrated over its area the magnetic flux  $\phi$  received is the total field over the integrated area [9]. The magnetic flux is described as

$$\begin{bmatrix} \phi_{as} \\ \phi_{bs} \\ \phi_{cs} \end{bmatrix} = L_s \begin{bmatrix} i_{as} \\ i_{as} \\ i_{as} \end{bmatrix} + L_{mag}^T \begin{bmatrix} i_{ar} \\ i_{br} \\ i_{cr} \end{bmatrix} \quad (11)$$

$$\begin{bmatrix} \phi_{ar} \\ \phi_{br} \\ \phi_{cr} \end{bmatrix} = L_r \begin{bmatrix} i_{ar} \\ i_{ar} \\ i_{ar} \end{bmatrix} + L_{mag}^T \begin{bmatrix} i_{as} \\ i_{bs} \\ i_{cs} \end{bmatrix} \quad (12)$$

where  $L$  is the circuit inductance with *mag* as subscript for magnetising inductances. The frequency of the current flowing in the rotor is not constant unless the rotor stands still. Therefore the inductance will vary according to (13), (14) and (15).

$$\bar{L}_s = \begin{bmatrix} L_{ls} + L_{mag} & -\frac{1}{2}L_{mag} & -\frac{1}{2}L_{mag} \\ -\frac{1}{2}L_{mag} & L_{ls} + L_{mag} & -\frac{1}{2}L_{mag} \\ -\frac{1}{2}L_{mag} & -\frac{1}{2}L_{mag} & L_{ls} + L_{mag} \end{bmatrix} \quad (13)$$

$$\bar{L}_r = \begin{bmatrix} L_{lr} + L_{mag} & -\frac{1}{2}L_{mag} & -\frac{1}{2}L_{mag} \\ -\frac{1}{2}L_{mag} & L_{lr} + L_{mag} & -\frac{1}{2}L_{mag} \\ -\frac{1}{2}L_{mag} & -\frac{1}{2}L_{mag} & L_{lr} + L_{mag} \end{bmatrix} \quad (14)$$

$$\bar{L}_{mag} = L_{mag} \begin{bmatrix} \cos(2\theta_r) & \cos(2\theta_r + \frac{2\pi}{3}) & \cos(2\theta_r - \frac{2\pi}{3}) \\ \cos(2\theta_r - \frac{2\pi}{3}) & \cos(2\theta_r) & \cos(2\theta_r + \frac{2\pi}{3}) \\ \cos(2\theta_r + \frac{2\pi}{3}) & \cos(2\theta_r - \frac{2\pi}{3}) & \cos(2\theta_r) \end{bmatrix} \quad (15)$$

where the subscript  $l$  denote leakage and  $\theta_r$  is the angular displacement of the rotors a phase  $a_r$  from the stators a phase  $a_s$  in Figure 9.  $\theta_r$  is shown in Figure 23.

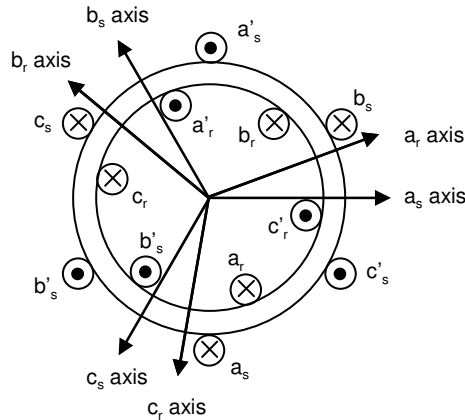


**Figure 9: Machine schematic**

The varying of the inductances is due to the angular displacement  $\theta_r$  of the rotor. The varying of the inductances will increase the mathematical complexity of the machine model [10]. To eliminate the time varying inductances and reduce the mathematical complexity of the machine model the variables in the stator and rotor associated with the three phase references frame a, b, c can be transformed into a common arbitrary reference frame called dq-frame. The dq reference frame is commonly fixed to the stator winding, the rotor winding or to a synchronously rotating quantity.

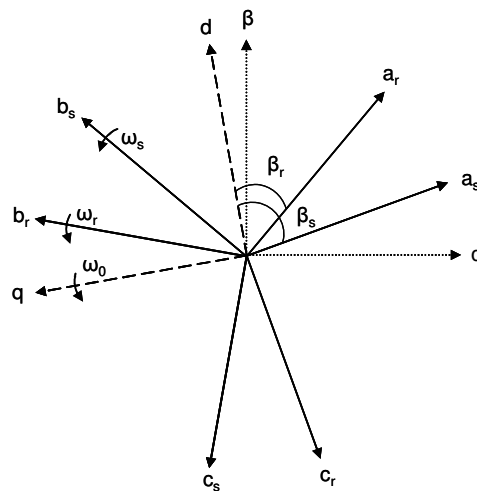


**Figure 10: Stator and rotor circuit frames and reference frames**

The a, b and c components are projected on to the d and q axes with Park’s transformation matrix:

$$T_{dq} = \sqrt{\frac{2}{3}} \begin{bmatrix} \cos(\beta) & \cos(\beta - \frac{2\pi}{3}) & \cos(\beta + \frac{2\pi}{3}) \\ -\sin(\beta) & -\sin(\beta - \frac{2\pi}{3}) & -\sin(\beta + \frac{2\pi}{3}) \end{bmatrix} \tag{16}$$

Transforming the stator three-phase system the  $\beta$  angle in the Park transformation equals the  $\beta_s$  angle and for the rotor the  $\beta_r$  angle in Figure 10. The Park’s transformation in (16) is valid under the assumption that the three-phase system is a symmetric system with the phases

shifted  $2\pi/3$ . Applying the transformation in Equation (16) on Equations (8), (9), (11) and (12) the voltage and flux can be rewritten in dq-frame according to:

$$\begin{bmatrix} v_{ds} \\ v_{qs} \end{bmatrix} = R_s \begin{bmatrix} i_{ds} \\ i_{qs} \end{bmatrix} + T_{dq}(\beta_s) \frac{d}{dt} (T_{dq}^{-1}(\beta_s) \begin{bmatrix} \varphi_{ds} \\ \varphi_{qs} \end{bmatrix}) \quad (17)$$

$$\begin{bmatrix} v_{dr} \\ v_{qr} \end{bmatrix} = R_r \begin{bmatrix} i_{dr} \\ i_{qr} \end{bmatrix} + T_{dq}(\beta_r) \frac{d}{dt} (T_{dq}^{-1}(\beta_r) \begin{bmatrix} \varphi_{dr} \\ \varphi_{qr} \end{bmatrix}) \quad (18)$$

$$\begin{bmatrix} \varphi_{ds} \\ \varphi_{qs} \end{bmatrix} = T_{dq}(\beta_s) L_s T_{dq}^{-1}(\beta_s) \begin{bmatrix} i_{ds} \\ i_{qs} \end{bmatrix} + T_{dq}(\beta_s) L_m T_{dq}^{-1}(\beta_r) \begin{bmatrix} i_{dr} \\ i_{qr} \end{bmatrix} \quad (19)$$

$$\begin{bmatrix} \varphi_{dr} \\ \varphi_{qr} \end{bmatrix} = T_{dq}(\beta_r) L_r T_{dq}^{-1}(\beta_r) \begin{bmatrix} i_{dr} \\ i_{qr} \end{bmatrix} + T_{dq}(\beta_r) L_m T_{dq}^{-1}(\beta_s) \begin{bmatrix} i_{ds} \\ i_{qs} \end{bmatrix} \quad (20)$$

Rewriting equations (17)-(20) gives:

$$\begin{bmatrix} v_{ds} \\ v_{qs} \end{bmatrix} = R_s \begin{bmatrix} i_{ds} \\ i_{qs} \end{bmatrix} + \frac{d}{dt} \begin{bmatrix} \varphi_{ds} \\ \varphi_{qs} \end{bmatrix} + \frac{d\beta_s}{dt} \begin{bmatrix} -\varphi_{qs} \\ \varphi_{ds} \end{bmatrix} \quad (21)$$

$$\begin{bmatrix} v_{dr} \\ v_{qr} \end{bmatrix} = R_r \begin{bmatrix} i_{dr} \\ i_{qr} \end{bmatrix} + \frac{d}{dt} \begin{bmatrix} \varphi_{dr} \\ \varphi_{qr} \end{bmatrix} + \frac{d\beta_r}{dt} \begin{bmatrix} -\varphi_{qr} \\ \varphi_{dr} \end{bmatrix} \quad (22)$$

$$\begin{bmatrix} \varphi_{ds} \\ \varphi_{qs} \end{bmatrix} = \begin{bmatrix} L_{ls} + \frac{3}{2} L_m & 0 \\ 0 & L_{ls} + \frac{3}{2} L_m \end{bmatrix} \begin{bmatrix} i_{ds} \\ i_{qs} \end{bmatrix} + \begin{bmatrix} \frac{3}{2} L_m & 0 \\ 0 & \frac{3}{2} L_m \end{bmatrix} \begin{bmatrix} i_{dr} \\ i_{qr} \end{bmatrix} \quad (23)$$

$$\begin{bmatrix} \varphi_{dr} \\ \varphi_{qr} \end{bmatrix} = \begin{bmatrix} L_{lr} + \frac{3}{2} L_m & 0 \\ 0 & L_{lr} + \frac{3}{2} L_m \end{bmatrix} \begin{bmatrix} i_{dr} \\ i_{qr} \end{bmatrix} + \begin{bmatrix} \frac{3}{2} L_m & 0 \\ 0 & \frac{3}{2} L_m \end{bmatrix} \begin{bmatrix} i_{ds} \\ i_{qs} \end{bmatrix} \quad (24)$$

The total generated power in a wind power turbine is the sum of the power in the rotor and the stator according to:

$$\begin{aligned} P_g &= (v_{as} i_{as} + v_{bs} i_{bs} + v_{cs} i_{cs}) + (v_{ar} i_{ar} + v_{br} i_{br} + v_{cr} i_{cr}) \\ &= (v_{ds} i_{ds} + v_{qs} i_{qs}) + (v_{dr} i_{dr} + v_{qr} i_{qr}) \end{aligned} \quad (25)$$

In the power balance for the DFIG all the power that is not lost or used to magnetizing the machine, is transferred power according to:

$$P_g = P_t - P_{loss} - P_{mag} \quad (26)$$

If the voltages in Equation (25) are expressed with equations (21) and (22) and the generated power with equation (26) the power balance can be expressed according to:

$$\begin{aligned} P_t - P_{loss} - P_{mag} &= \\ &= R_s (i_{ds}^2 + i_{qs}^2) + R_r (i_{dr}^2 + i_{qr}^2) \\ &+ \frac{d\varphi_{ds}}{dt} i_{ds} + \frac{d\varphi_{qs}}{dt} i_{qs} + \frac{d\varphi_{dr}}{dt} i_{dr} + \frac{d\varphi_{qr}}{dt} i_{qr} \\ &+ \frac{d\beta_s}{dt} (-\varphi_{qs} i_{ds} + \varphi_{ds} i_{qs}) + \frac{d\beta_r}{dt} (-\varphi_{qr} i_{dr} + \varphi_{dr} i_{qr}) \end{aligned} \quad (27)$$

From equation (27) the transferred, the lost and the magnetizing power can be identified as:

$$P_t = \frac{d\beta_s}{dt} (-\varphi_{qs} i_{ds} + \varphi_{ds} i_{qs}) + \frac{d\beta_r}{dt} (-\varphi_{qr} i_{dr} + \varphi_{dr} i_{qr}) \quad (28)$$

$$P_{loss} = -(R_s (i_{ds}^2 + i_{qs}^2) + R_r (i_{dr}^2 + i_{qr}^2)) \quad (29)$$

$$P_{mag} = -\left(\frac{d\varphi_{ds}}{dt}i_{ds} + \frac{d\varphi_{qs}}{dt}i_{qs} + \frac{d\varphi_{dr}}{dt}i_{dr} + \frac{d\varphi_{qr}}{dt}i_{qr}\right) \quad (30)$$

The electromagnetic torque can be expressed as

$$T_e = \frac{P_t}{\omega_m} = \frac{1}{\omega_m} \left(\frac{d\beta_s}{dt}(-\varphi_{qs}i_{ds} + \varphi_{ds}i_{qs}) + \frac{d\beta_r}{dt}(-\varphi_{qr}i_{dr} + \varphi_{dr}i_{qr})\right) \quad (31)$$

### 3.4.2 Mechanical dynamics

The mechanical dynamics of a machine can be described as

$$J \frac{d\omega_m}{dt} = (T_m - T_e) \quad (32)$$

Where  $J$  is inertia of the machine,  $T_m$  and  $T_e$  is mechanical and electromagnetic torque. In wind power turbines the inertia is often defined in a per unit system according to:

$$H = \frac{J\omega_n^2}{2S_n} \quad (33)$$

where  $H$  is the inertia constant of the shaft and generator in seconds,  $S_n$  is the rated power and

$$\omega_n = \frac{\omega_s}{p} \quad (34)$$

where  $\omega_s$  is the synchronous speed and  $p$  is the number of pole pairs.

## 3.5 Converter

As stated before the rotor power passes through a back to back converter. The converter controls the frequency of the current to the rotor and the converter power on the grid side to be pure active. There are many papers about back to back converters and pulse width modulated rectifiers; I will give a description based on the information found in [12].

### 3.5.1 Pulse width modulated converter

The back to back converter consists of one Pulse Width Modulated (PWM) rectifier and one inverted PWM rectifier with a DC-link capacitor in between as shown in Figure 11. The only difference between the inverter and rectifier is the definition of the power sign. The rotor side of the converter is modulated to give a sinusoidal line current with a chosen frequency. The DC-link voltage is regulated and kept constant by controlling the power flow through the grid side of the converter. The rectifier and inverter consists of three transistor half-bridges each built up by semiconductors, see Figure 11.

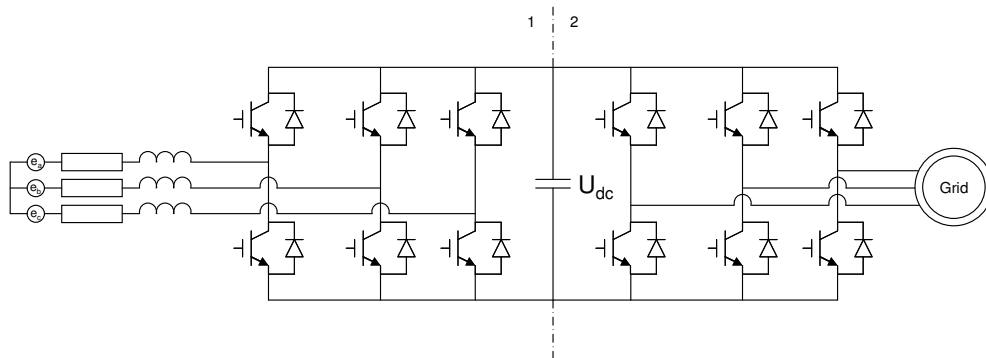
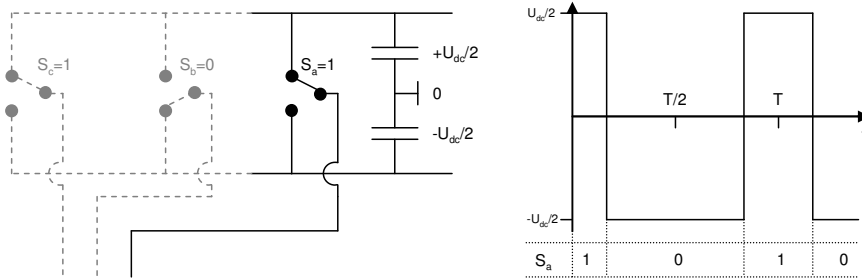


Figure 11: Back to back converter with transistor half-bridges

Voltage modulation means that the momentary output voltage alters between two well defined voltage levels. A transistor half-bridge represent a switch and a PWM rectifier has three switches  $\{s_a s_b s_c\}$ . The switches are either high or low and therefore the phase potential for each line is modulated between  $\pm U_{dc}/2$  as show in Figure 12.



**Figure 12: Converter switch and output line voltage for one phase**

The difference between the line voltages create the phase voltage output from the converter expressed as:

$$\begin{aligned} u_{ab} &= u_a - u_b \\ u_{ac} &= u_a - u_c \\ u_{bc} &= u_b - u_c \end{aligned} \tag{35}$$

The phase voltage is  $\pm U_{dc}$  or 0V while the line voltages alter between  $\pm U_{dc}/2$ . Applying Kirchoff’s voltage law on the left side of Figure 11 gives:

$$\begin{aligned} L \frac{di_a}{dt} - e_a + u_a - Ri_a &= 0 \\ L \frac{di_b}{dt} - e_b + u_b - Ri_b &= 0 \\ L \frac{di_c}{dt} - e_c + u_c - Ri_c &= 0 \end{aligned} \tag{36}$$

where  $e$  is the phase voltage. Assuming that the switching frequency period time is much longer than the inductive time constant  $L/R$  in the rotor and the rotor losses can be neglected the phase current in (36) can be approximated to:

$$\begin{aligned} \Delta i_a &= \frac{1}{L}(e_a - u_a)\Delta t \\ \Delta i_b &= \frac{1}{L}(e_b - u_b)\Delta t \\ \Delta i_c &= \frac{1}{L}(e_c - u_c)\Delta t \end{aligned} \tag{37}$$

In Equation (35) it is concluded that the phase voltage can be controlled by independently controlling the switches  $\{s_a s_b s_c\}$  and in (37) it is concluded that if the output voltage is controlled the current from the converter can be controlled.

The “DFIG controller” discussed in Chapter (3.3) calculates the average voltage  $\{u_a u_b u_c\}$  for each phase and switching period based on its reference values. The switching period is the time it takes for a semiconductor to switch from one state and back again. The pulse width of the modulated line voltage must be controlled to equal the calculated average voltage. This is done by comparing the average voltage reference with a carrier wave. This can be seen in Figure 13 for one phase with the constant reference value  $u_{a,ref}$ . The carrier use a triangular wave as it gives less current ripple compared to other carrier waves. If the

reference value is higher than the carrier wave the switch shown in Figure 12 is  $s=1$  and if it is below the switch  $s=0$ .

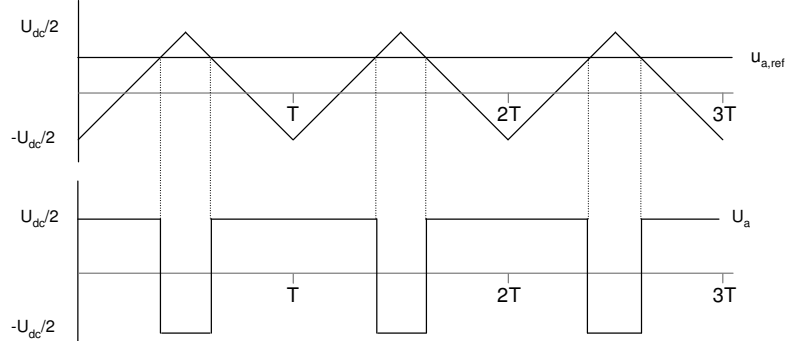


**Figure 13: Converter modulation and voltage output for one phase**

Modulating a three phase converter the line reference  $u_{a,ref}$  in Figure 13 and for the other two phases is original a sinusoidal. The sinusoidal reference can be altered with a so called zero sequence component to increase the voltage output from the controller. Controlling with a pure sinusoidal i.e. a sinusoidal that has not been altered with a zero sequence the references are:

$$\begin{aligned}
 u_{a,ref} &= \hat{u} \sin(\omega t) \\
 u_{b,ref} &= \hat{u} \sin(\omega t + \frac{2\pi}{3}) \\
 u_{c,ref} &= \hat{u} \sin(\omega t + \frac{4\pi}{3})
 \end{aligned}
 \tag{38}$$

For a sinusoidal reference the voltage amplitude  $\hat{u}$  can be set between 0 and  $U_{dc}/2$ . If it is set above  $U_{dc}/2$  the peak values of the reference sinusoidal is above the maximum output voltage available from the DC-link and the output signal cannot obey the reference. This is called over modulation. When modulating with sinusoidal reference the maximum use of the DC link capacitors voltage is 78%, meaning that the line output voltage from the converters is  $\pm U_{dc}$  78% of a switching period and 0V 22% of the period. By adding a zero sequence signal to the original sinusoidal signal the use of the DC-link voltage can be increased. For symmetrical reference the zero-sequence signal is calculated from

$$u_z = \frac{1}{2} (\max(u_{a,ref}, u_{b,ref}, u_{c,ref}) + \min(u_{a,ref}, u_{b,ref}, u_{c,ref}))
 \tag{39}$$

The line reference is the changed according to:

$$\begin{aligned}
 u_{az,ref} &= u_{a,ref} - u_z \\
 u_{bz,ref} &= u_{b,ref} - u_z \\
 u_{cz,ref} &= u_{c,ref} - u_z
 \end{aligned}
 \tag{40}$$

The maximum voltage amplitude  $\hat{u}$  for a sinusoidal reference with a symmetric zero sequence added is:

$$\hat{u} = \frac{1}{\sqrt{3}} U_{dc}
 \tag{41}$$

The sinusoidal and the symmetrical reference is shown in Figure 14 for  $U_{dc}=400V$  and  $f=50Hz$ .  $\hat{u}$  is increased from  $U_{dc}/2$  to  $U_{dc}/\sqrt{3}$  for the symmetrical modulation and increasing the DC-link voltage utilization about 15%.

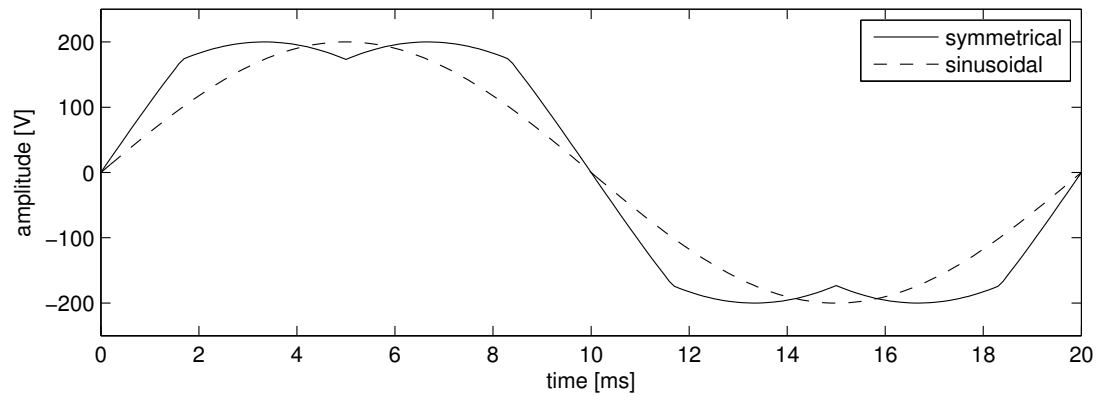


**Figure 14: Symmetrical and sinusoidal modulation**



## 4 Operational situations

A wind power turbine has a number of different operational situations it can be exposed to. Different operational situations cause different forces on the power turbine. Therefore measurements are done for different situations and are to be studied. The situations are described below and are a summary of [13].

### 4.1 Normal Production

Normal production is optimal production without any limitation by external reference.

### 4.2 Curtailment

Electrical power production is a combination of different power sources such as wind, water, coal and nuclear. Electricity can not be stored in an efficient way today, therefore it is essential that there is equilibrium between produced and consumed electricity. If the request for electricity is low and the production capacity is high the price per energy unit is low. If the difference is very big the power producer is charged to distribute the electricity if their production capacity can not be decreased. In countries where hydropower is a big part of the power production it is easy to regulate the power production. In countries with coal and nuclear as dominating production sources it is harder to regulate the power production due to the characteristics of the turbines. Therefore it is of interest to control the output power from wind power turbine. This is called curtailment.

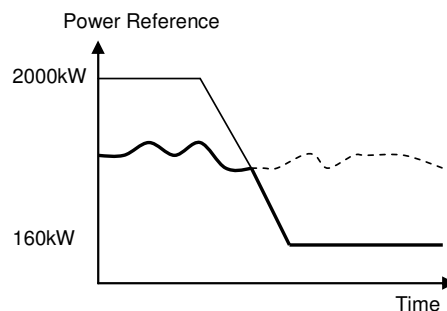


**Figure 15: Curtailment**

In Figure 15 an example of curtailment can be seen. The grey line is from the operators, requested output, the black line is the actual output, the dotted line is the possible power production and the difference between the black and dotted line is the available production. The power reference for a single wind power turbine is set according to the demanded total power production from the wind park. Default is maximum production.

### 4.3 Normal Stop

It is required to be able to stop wind power turbines for different reasons such as maintenance. Under a normal stop the power is ramped down during a couple of second and then the wind power turbine is stopped and disconnected.

### 4.4 Emergency Stop

There are some different trigger levels in a power turbine that causes emergency stop. It can for example be over speed, generator failure or fire. When trigger levels are reached the blades are pitched to a maximum against the wind and the turbine is braked to a full stop.

The turbine is going from production to a full stop in about two seconds. It is also possible to hit an emergency button and initialize an emergency stop manually.

#### 4.5 Star/ $\Delta$ Switch

The star/ $\Delta$  switch is a physical change in the electrical connection between the rotor and transformer. The star connection has a zero-reference compared to the  $\Delta$  connection as shown in Figure 16.

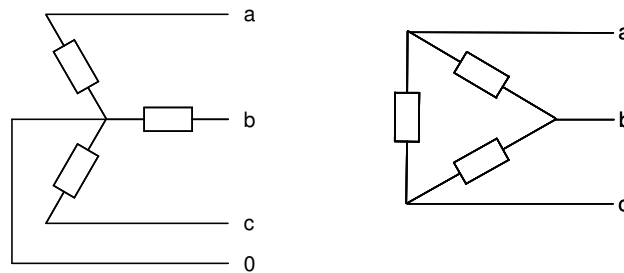


**Figure 16: Star (left) and  $\Delta$  (right) connection**

In the  $\Delta$  connection the phase and line voltage is the same in difference to the star connection where the line voltage is the square root of three higher than the phase voltage.

$$U_{y,line} = \sqrt{3}U_{y,phase} \quad (42)$$

$$i_{y,line} = i_{y,phase}$$

The line and phase current is the same in the star connection. In the  $\Delta$  connection the phase current is the square root of three higher for the line current.

$$U_{\Delta,line} = U_{\Delta,phase} \quad (43)$$

$$i_{\Delta,line} = \sqrt{3}i_{\Delta,phase}$$

The  $\Delta$  connection has a high current but a low voltage while the star connection has a high voltage and a low current. The generator do not have to produce the same amount of energy for star connection as  $\Delta$  connection to keep the voltage at 690V. The electromagnetic torque is also decreased so the turbine can produce power at lower wind speed. 690V is commonly the output voltage from the stator.

The trigger levels may vary for different wind power plans but generally the star  $\rightarrow$   $\Delta$  switch is done when the power production has been above 500kW for longer than 15s. After 15s the power is automatically reduced to 0kW and the physical switch from star to delta connection is done. Then the power is ramped up again. For star connection the maximum production is 950kW. The  $\Delta \rightarrow$  star switching is done in the same way, but instead when the power production has been less than 250 kW for 15 seconds. The power is reduced to 0kW and the switching to star connection is done before the power is ramped up again.

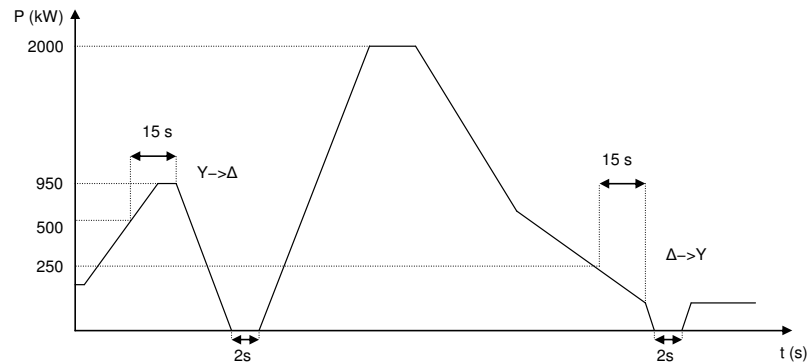


Figure 17: Star/Δ switch

#### 4.6 Over Speed

The wind turbines are regularly checked and pre-emptive maintenance is done. To ensure that the safety system works properly during the maintenance an over speed test is done. During the test the blades are pitched so the rotor is slowly accelerated up from 0 to 1950 rpm. When the speed hits 1950 rpm an emergency stop is performed. This is done without any power production.

#### 4.7 Start Up

The turbine is slowly ramped up from full stop. When reached normal production the turbine is connected to the power grid.

#### 4.8 Idling

The wind power turbine runs without any load, without the generator magnetized.



### 5.1.3 Mechanical setup

A number of different mechanical measurements are done at different sampling frequencies [17]. For this thesis the torque measurement on the high speed shaft is of main interest.

Some of the measurements done seen in Figure 19 are:

#### High sample rate -250kHz

Signal	Unit
Torque HSS & LSS	Nm
Bending HSS& LSS	Nm
Acceleration HSS	G

#### Medium sample rate- 2.5kHz

Signal	Unit
Displacement X &Y, HSS & LSS	mm

where HSS is the high speed shaft, the LSS low speed shaft.

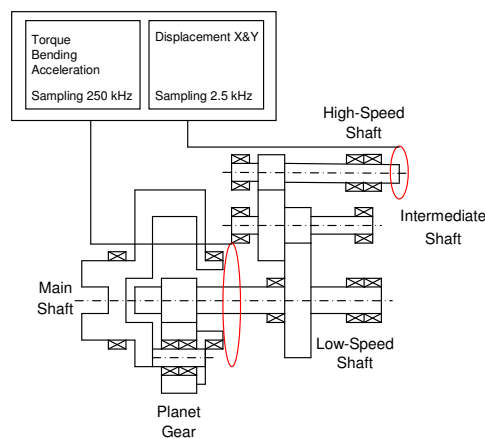


**Figure 19: Gearbox measurements**

The bending of the HSS and LSS – shaft is the axial bending measured with strain gauges. The displacement in X and Y is how much the gearbox is displaced where the HSS and LSS shafts are connected.

### 5.1.4 Measurement limitation

The intention was to do the electrical and mechanical measurements at the same time and synchronize them with a GPS time signal. Unfortunately the mechanical setup did not work during the measurements and this was first discovered after the electrical setup was disassembled. Due to high cost for the electrical setup the measurement equipment was not put back for the retake of the mechanical measurements. Therefore the measurements are done for the same scenarios but on different times.

The rotor angle in the electrical measurements has been corrupted for a large amount of the measurements i.e. something gone wrong with the measurement equipment so the speed measurements are not accurate. This limits the amount of data that can be used in this thesis.

For the mechanical measurement there is a scaling error and an offset error. The size of the scaling and offset error is unknown for this Thesis. But it can be assumed that the measured mechanical torque gives a sufficient picture of the torque characteristic.

## 5.2 Data Processing

A part of this thesis has been to process the electrical data to a format that can be used by MATLAB. A sampled rate of 44.1 kHz for a couple of hours gives a lot of data to process. The electrical data was sampled by a program called powerLab in files with periods of one minute. With a data converter the files were transferred from the powerLab format to .tdms format. National Instrument has developed a script reading .tdms files into MATLABs workspace [18]. This script was modified to read the .tdms files and save the powerLab and SCADA measurements in MATLABs .mat format. In addition to the current, voltage and speed measurements as earlier mentioned there is also GPS time sync and analogue speed saved in the files. This data have also been collected in the measurements. The GPS data was supposed to be used to synchronize the mechanical and electrical measurements and the analogue speed is calculated in powerLab from the digital speed measurements the black and white tape gave. How the analogue speed is calculated is unknown and therefore it is not used in the model. From the digital speed measurements the stator and rotor angles in Figure 10 are calculated according to (5.2.1) and (5.2.2) for this Thesis.

### 5.2.1 Stator angle

The synchronous velocity for the d/q frame can be chosen arbitrary as discussed in Chapter (3.4.1). In this thesis we chose the synchronous d-axis velocity to coincide with the magnetic flux in the stator according to Figure 20 and the stator a-phase to coincide with the  $\alpha$ -axis in the  $\alpha/\beta$ -frame shown in Figure 10. The choice of the synchronous speed is because the magnetic flux rotates with the same frequency as the grid frequency and the grid frequency is fairly constant. Therefore is it natural to use it as the synchronous frequency.

The voltage vector in  $\alpha/\beta$ -frame can be calculated according to:

$$\vec{e}^{\alpha\beta} = \sqrt{\frac{2}{3}}(e_a + e_b e^{j\frac{2\pi}{3}} + e_c e^{j\frac{4\pi}{3}}) = E e^{j\omega t} \quad (44)$$

In (7) it is derived that integrating the magnetic flux gives the voltage. Integrating the voltage vector gives the magnetic flux in  $\alpha/\beta$ -frame:

$$\vec{\varphi}_s = \int E e^{\alpha\beta} dt = \frac{E}{\omega} e^{j(\omega t - \frac{\pi}{2})} \quad (45)$$

In Equation (44) and (45) it can be seen that the magnetic flux  $\varphi$  is rotating with the same speed as the voltage vector lagging  $\pi/2$  radians behind.

With Equation (44) the voltage vector for every sample can be calculated. Calculating the  $\alpha$  and  $\beta$  part of the voltage vector the angle  $\beta_s$  can be calculated with:

$$\beta_s + \frac{\pi}{2} = \arctan\left(\frac{\beta}{\alpha}\right) \quad (46)$$

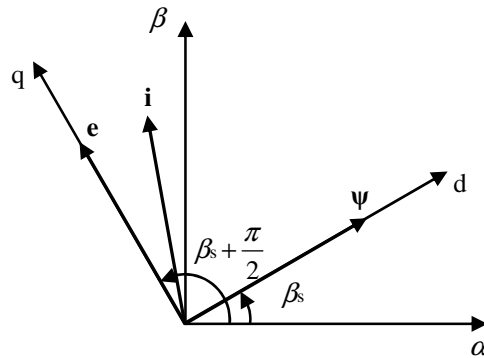


Figure 20: Stator frames

5.2.2 Rotor angle

The rotor angle must be calculated from the pulse train seen in Figure 21 made by the black and white tape. There are 32 high pulses and one discontinuity caused by the black and white tape not joined together exactly at 32 equally high pulses in every revolution as shown in Figure 21. Knowing this it is possible to calculate the number of samples in the revolutions. If the speed is assumed to be constant during the same revolution the linear gradient  $k$  for the angle increase can be calculated according to:

$$k = \frac{2\pi}{\text{number of sample/revolution}} \tag{47}$$

With the straight-line equation the angle for every sample can then be calculated if the initial angle is known.

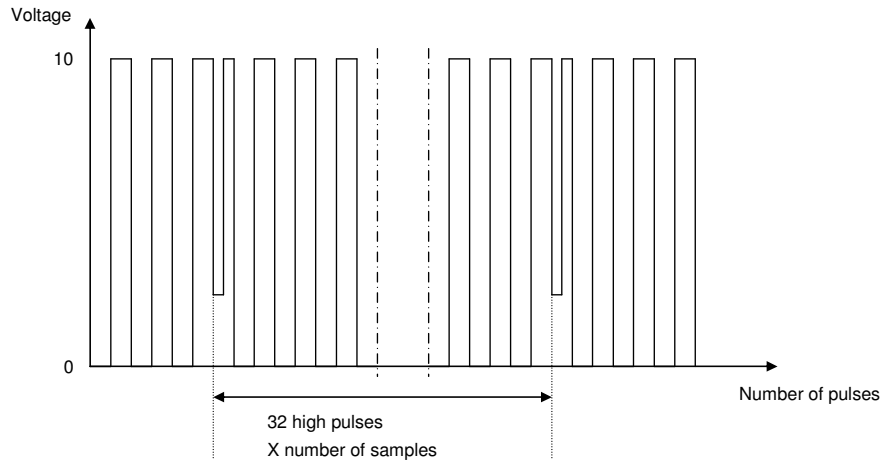
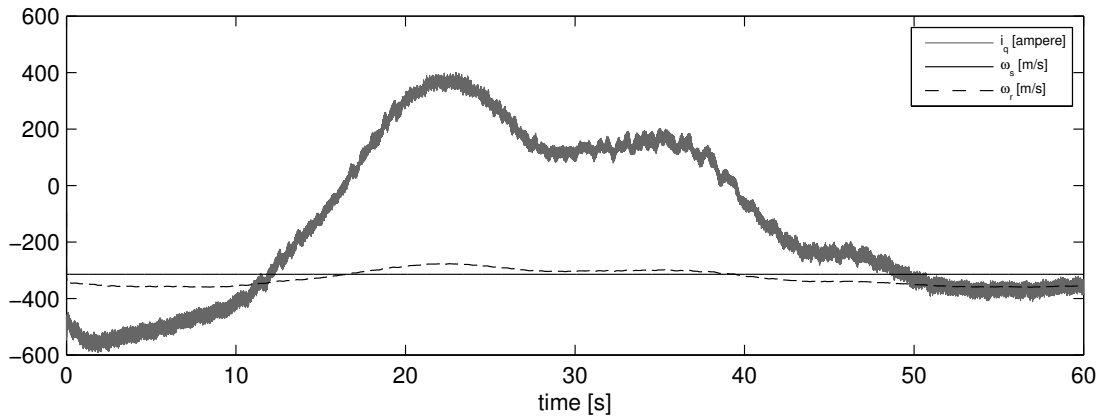


Figure 21: Pulse train for rotor speed

In Chapter (3.2) it is discussed that the rotor consumes power in sub synchronous speed and produce power in super synchronous speed and therefore the rotors current on the q-axis changes sign when the rotor speed passes the synchronous speed as shown in Figure 22.



**Figure 22: Rotor q-current when rotor speed passes the synchronous speed**

From the sign change, the rotor and the synchronous speed the initial angle between the a-phase coil and the  $\alpha$ -axis can be calculated. By iterate the initial angle between  $[0 \ 2\pi]$  it is possible to find the angle for the q-axis when it changes sign at the same time as the rotor speed passes the synchronous speed. In Figure 35 it can be seen how the q-current is changed for the initial angle. In Figure 22 it can be seen that for 16s and 39s the rotor passes the synchronous and the q-current changes sign at the same instant.

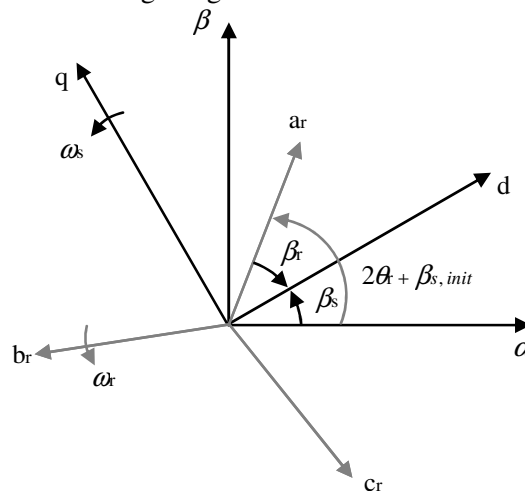


**Figure 23: Rotor frames**

The angle calculated is the  $\theta_r$  angle. The desired angle in Equation (16) is calculated from:

$$\beta_r = 2\theta_r - \beta_s + \beta_{r,init} \tag{48}$$

### 5.2.3 Velocity and acceleration

In Chapter (5.2.1) and (5.2.2) the angles for the rotor and stator are calculated. By numerical derivation the angular speed is calculated according to Equation (49). The second differentiate of the mechanical angle gives us the rotor acceleration according to Equation (50).

$$\omega = \frac{d\beta}{dt} \tag{49}$$

$$a = \frac{d\omega}{dt} \tag{50}$$



### 5.3 Model

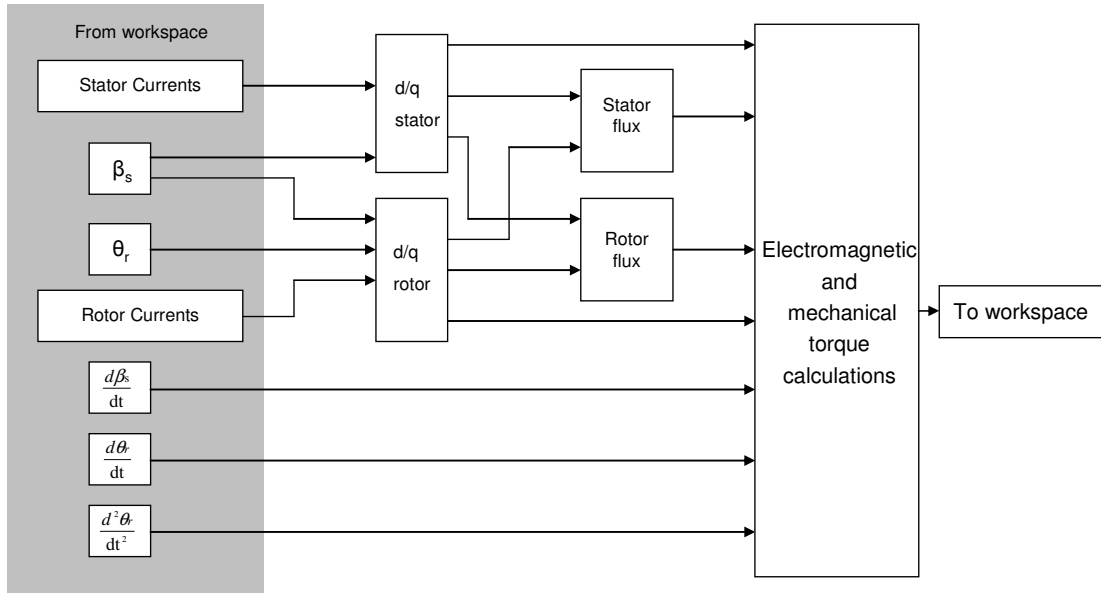


**Figure 24: Schematic picture of model**

The Simulink model calculates the mechanical torque according to the mathematical theory in Chapter (3.4.1). A schematic picture of the MATLAB/Simulink model is shown in Figure 24 and the simulation block diagrams are shown in Appendix A. The inputs to the model are the stator and rotor a, b and c phase currents and the angles, velocities and acceleration calculated according to Chapter (5.2). Simulink imports these data from MATLABs workspace in which the different data first needs to be loaded. This is done with an m-file called “simfile”, seen in Appendix B. The same m-file runs the simulation and plots the simulated mechanical torque. When the simulation is running the d/q blocks transforms the rotor and stator current into d/q quantities according to Park’s transformation in Equation (16). With the inductance and the current in d/q-frame the stator and rotor flux can be simulated in respective block according to Equation (23) and (24). The inductance parameters can be found in Table 1 together with the inertia constant H. With the transformations done and the flux simulated the electromagnetic torque in Equation (31) and the mechanical torque in Equation (32) can be calculated in the calculation block. When the simulations are done the mechanical torque is exported to MATLABs workspace and plotted by the “simfile”.

#### 5.3.1 Parameters

To calculate the stator and rotor flux in Equations (23) and (24) the leakage inductances in the rotor and stator and the magnetic leakage inductance are required. The inductance in the test wind power turbine is not available because of confidentiality. In [20] the parameter for an arbitrary wind power turbine of the same size for the one used in this Thesis are found. To calculate the moment of inertia in Equation (33) the inertia constant H of the shaft and generator in seconds is needed. This can also be found in [20]. The generator parameters used can be seen in Table 1.

H	3.5	[s]
Lm	$3 \cdot 10^{-3}$	[H]
Ls	$72.9 \cdot 10^{-6}$	[H]
Lr	$372 \cdot 10^{-6}$	[H]

**Table 1: Generator parameters**

## 5.4 Simulation Signals

In this Chapter the different signals in the model are visualised. The data used in the model is sampled with 44.1 kHz. In .mat format the size of the collected data becomes big. To be able to simulate a whole minute without overflowing a normal laptop's memory the simulations have to be down sampled to at least every second sample. In this thesis the measurements are down sampled 10 times. This gives a fast simulation time and a sufficient resolution.

### 5.4.1 Stator current

The inputs to the Simulink model described in Chapter (5.3) from the stator are the phase current. In Figure 25 the current for phase "a" is shown for the curtailment run scenario with the power reference set to 400kW.

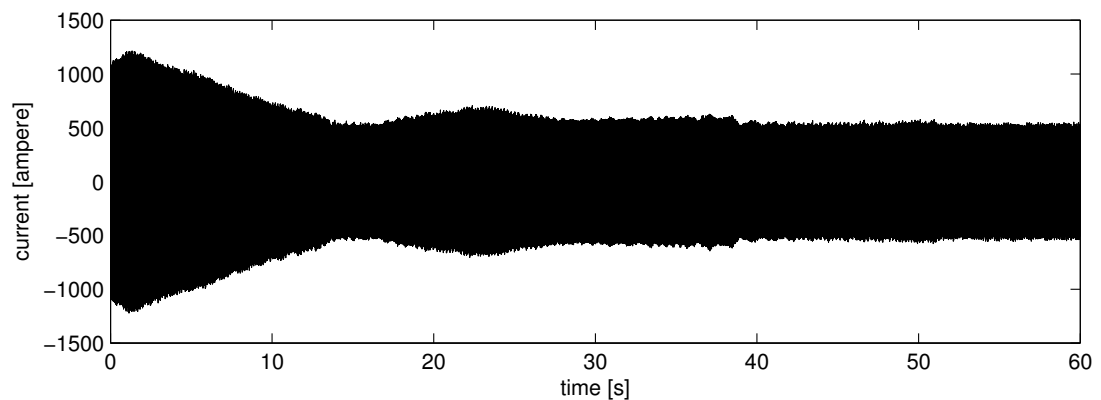


**Figure 25: Stator current in phase a**

When transferred to d/q-frame the synchronous reference is chosen according to Chapter (5.2.1). The stator current in d/q frame are shown in Figure 26.

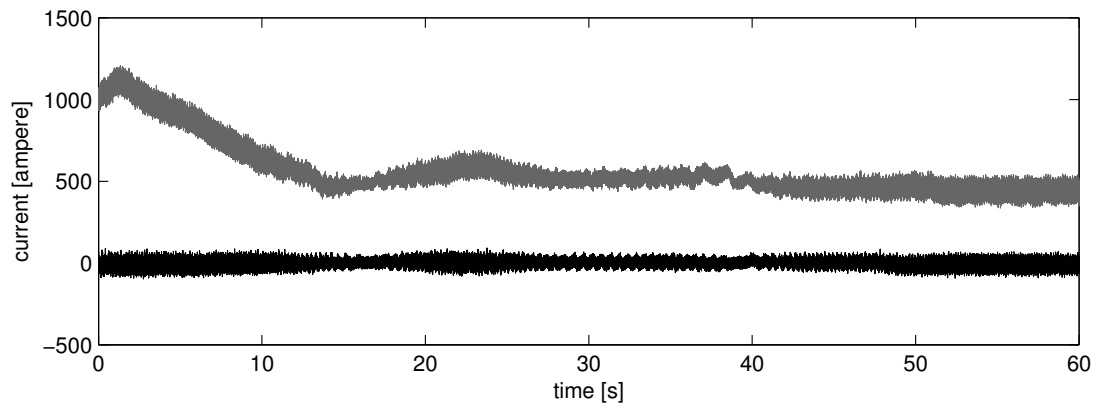


**Figure 26: Stator current in d (black) and q (grey) reference frame with stator flux as synchronous reference.**

#### 5.4.2 Rotor current

The rotor current for phase “a” used in the model in Chapter (5.3) is shown in Figure 27 for the run scenario normal production.

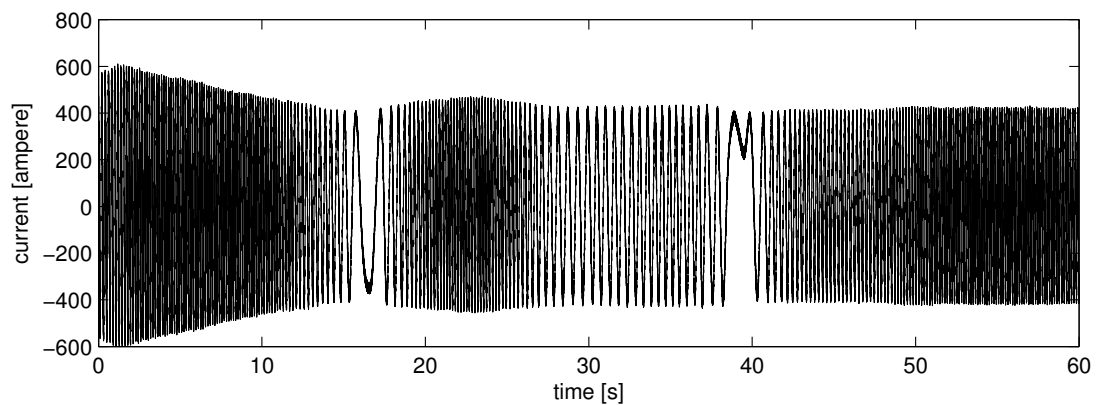


**Figure 27: Rotor current in phase a**

For the same synchronous reference frame as for the stator the d/q current are shown in Figure 28.

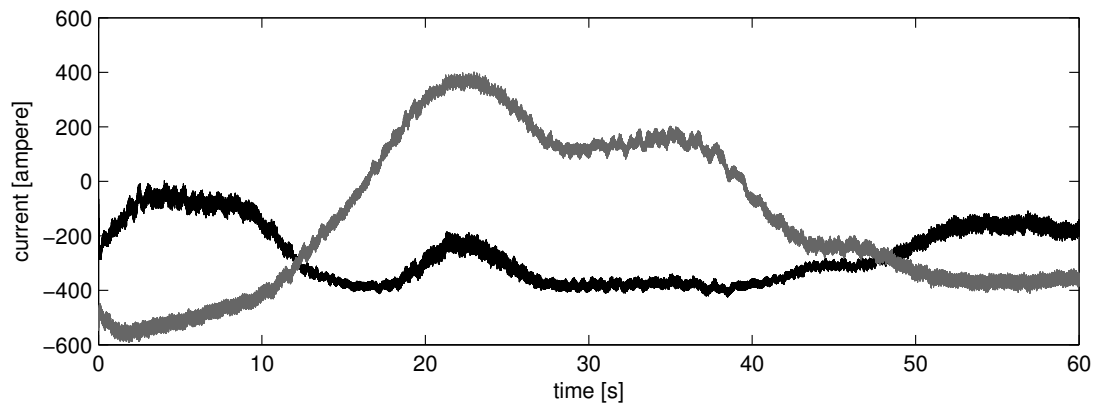


**Figure 28: Rotor current in d (black) and q (grey) reference frame with stator flux as synchronous reference.**

In Chapter (3.5.1) the converter and symmetrical modulation is discussed. The rotor voltage is modulated with a PWM-converter, meaning the output from the converter is well defined to  $\pm U_{dc}$  or  $0V$ . The inductance in the rotor circuit reduces the pulses and makes the signal more sinusoidal. If the signal is low pass filtered the converter modulation characteristics can be seen. Low pass filtering the voltage in phase “a” with the cut off frequency of 35 Hz and down sample the measured rotor voltage 1/500 times the original sample frequency with the MATLAB command “decimate” the result can be seen in Figure 29. In Figure 14 both sinusoidal and symmetrical simulation can be seen. Comparing the signals in Figure 14 and Figure 29 it can clearly be seen that the converter for the wind turbine in this thesis have the characteristics of symmetrical simulation. By using symmetrical simulation the utilization of the DC link capacitor is increased compared to sinusoidal modulation.

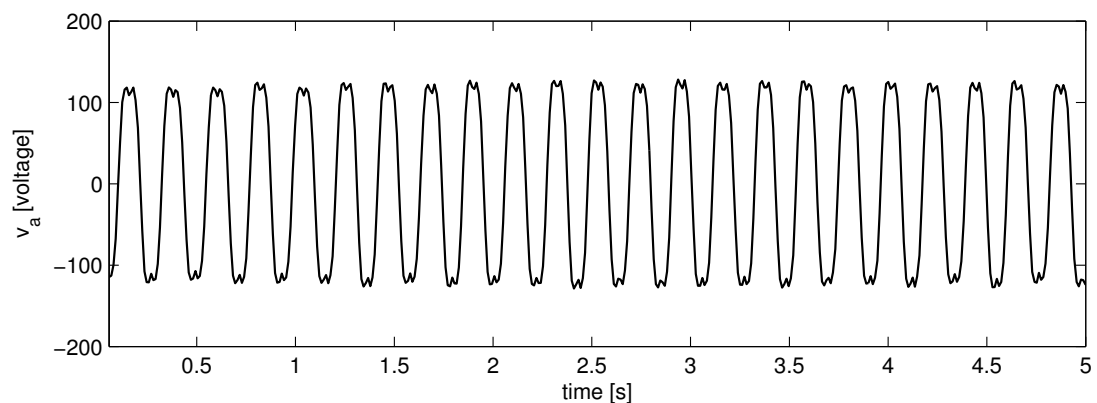


**Figure 29: Rotor voltage phase “a” down sampled and filtered**

It is discussed in Chapter (3.2) that the rotor is consuming power in sub synchronous speed and produce power in super synchronous speed. In Figure 30 the rotor power is plotted together with the rotor and stator speed. It can be seen in the figure that when the rotor speed goes below the synchronous speed after approximately 20 seconds the rotor starts consuming power and does so until the rotor goes above the synchronous speed again after 40 seconds.

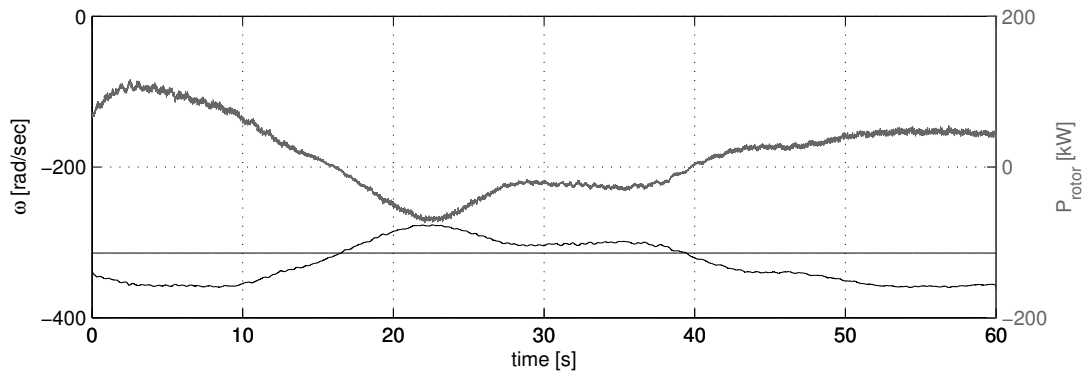


**Figure 30: Rotor Power (grey) and the rotor and stator speed (black)**

#### 5.4.3 Angle, velocity and acceleration

In Chapter (5.2.2) the rotor angle is calculated. The tape on the rotor is not placed in a protected environment therefore detection of the high and low pulses will be subject to noise in form of e.g. dirt on the tape. This is reflected on the pulse train. To easier count the high and low pulses and calculate the angle the signal is filtered with a 1<sup>st</sup> order Butterworth low pass filter with the cut off frequency of 3.3 kHz. In one revolution the black and white tape gives rise to 32 high pulses. If the mechanical frequency of the rotor is 25 Hz the frequency of the pulse train is 0.8 kHz. This gives a good margin and high frequency noisy is excluded by the filter. The filtered signal is shown in Figure 31.

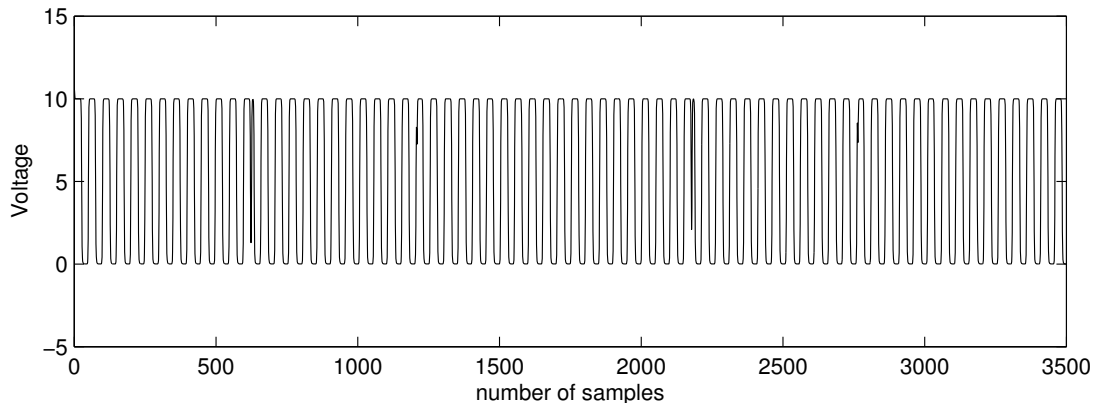


**Figure 31: Pulse train from black and white tape around rotor**

Torque calculations are sensitive to measurement errors in the recorded angle. A constant measurement error in the size of 0.2 ‰ gives a consistent error in the calculated torque. As shown in Figure 32. This demands a high accuracy on the measurement equipment.

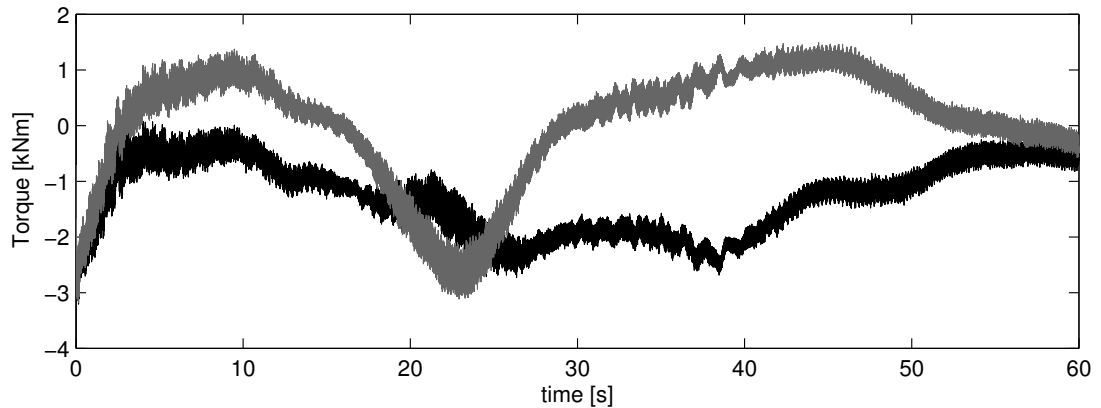


**Figure 32: Torque calculated in model (black) and torque calculated with 0.2% measurement error.**

The stator angle calculated with Equation (46) is in the interval  $[-\pi, \pi]$  while the rotor angle  $\theta_r$  is in the interval  $[-\pi, (\pi + 2\pi \cdot n)]$  where  $n$  is the number of revolutions. To calculate  $\beta_r$  in Equation (48) the rotor angle  $\theta_r$  and the stator angle  $\beta_s$  must be in the same interval. If the angles are in the interval  $[-\pi, \pi]$  there will be a step in the angle once a revolution between  $-\pi$  and  $\pi$  when the angle hits  $\pi$ . This will lead to high spikes when the angles are differentiated into speed. Therefore the stator angle is recalculated to the same interval as the rotor,  $[-\pi, (\pi + 2\pi \cdot n)]$ . This is done with the MATLAB command “unwrap”. There is still noise after the stator angle is differentiated into speed. Therefore the stator velocity is filtered with a 1<sup>st</sup> order Butterworth filter with the cut off frequency of 0.7 Hz. The filter with the cut off frequency of 0.7 Hz is only excluding undesired high frequency noise. The stator speed calculated from the grid frequency has slow frequency changes. In Figure 33 the stator and rotor velocity are shown.

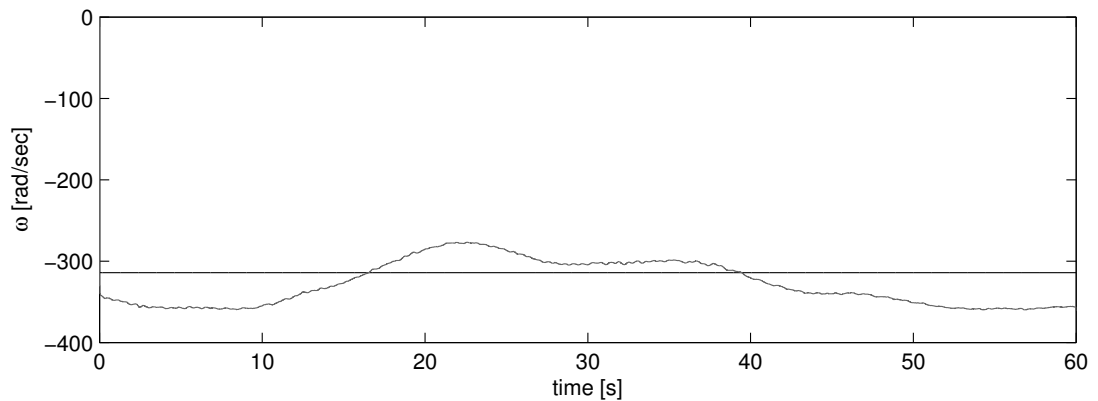


**Figure 33: Angular velocity of stator flux (black) and electrical rotor speed (grey)**

The angular acceleration of the rotor is the second derivative of the rotor angle. When differentiated once to obtain the speed the signal is good. When differentiated a second time to obtain the acceleration the signal gets noisy and has to be filtered. It is filtered with the same filter as for the stator velocity. The rotor acceleration is shown in Figure 34.

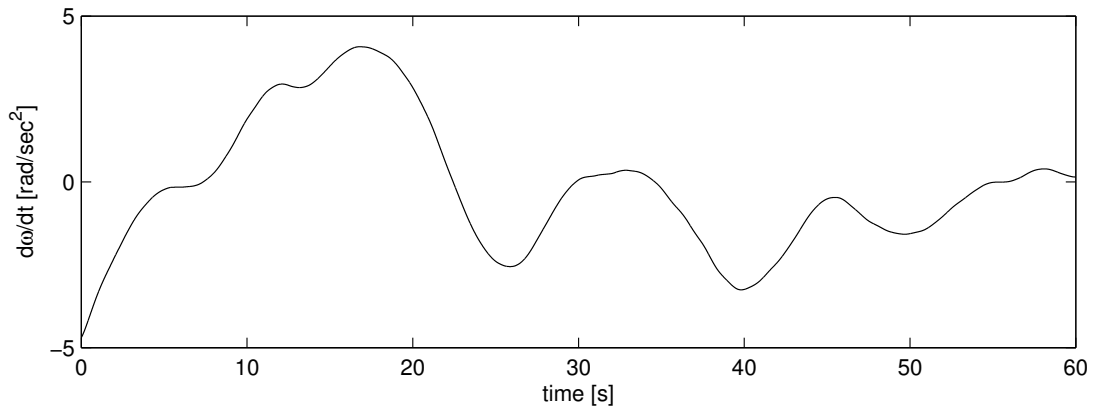


**Figure 34: Angular acceleration of the rotor**

The initial angle for the rotor is discussed in Chapter (5.2.2). In Figure 22 it can be seen when the rotor crosses the synchronous speed and the q-current changes sign. Comparing those two graphs the initial angle can be decided. In Figure 35 the q-current for three different initial angles can be seen with a difference off  $\pi/8$  rad. It is easy to find the initial angle roughly but more exactly it can be hard to decide. In the case for Figure 35 the initial angle  $\beta_{s,init}$  is 2.38 rad. In this Thesis the initial angle have to be iterated for each file. In Chapter (5.2.2) it is also discussed that there is a discontinuity in the pulse train due to the black and white tape is not joined together at exactly 32 high pulses. This discontinuity can be used to find the initial angle automatic. The number of pulses before the first discontinuity corresponds to the initial angle. The initial angle requires calibration down to the tenths of a radian. This makes it hard to automate the calculation of the initial angle exact enough and has not been done for this Thesis.

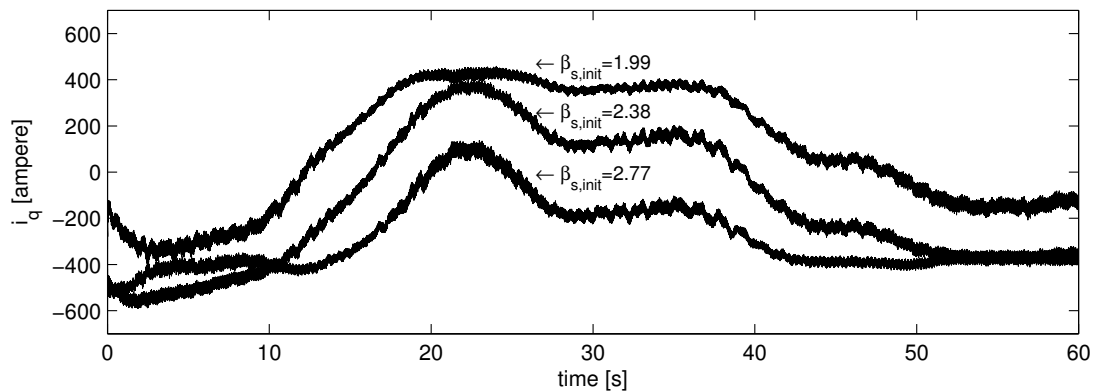


**Figure 35: Rotor  $i_q$  current for different initial angles  $\beta_s$ .**

## 6 Analysis and Results

The purpose with the Master Thesis is to conclude if the measured data can be used to gain new knowledge about wind power and wind power breakdown. The goal is to build a model that simulates the mechanical torque from the electrical measurements. There have been two aspects of the thesis. First isolate the different run scenarios in the measurements and briefly analyse them. The second part to build the model that calculates the corresponding mechanical torque generated by the wind based on the electrical measurements.

### 6.1 Electrical Measurements

One reason for the electrical measurements is that different scenarios can lead to electrical transients and that these can impose unexpected load scenarios [13]. Those transients could be caused by pitch and converter algorithms or external regulation. The run scenarios have been isolated, plotted and analysed ocular to see if there was any obvious unexpected transient in the measurements. This was also done to increase knowledge about induction machines and what happens at different scenarios.

The different run scenarios isolated is described in Chapter 4. The analysis was done from the SCADA data, the rotor and stator current and voltage and the analogue speed.

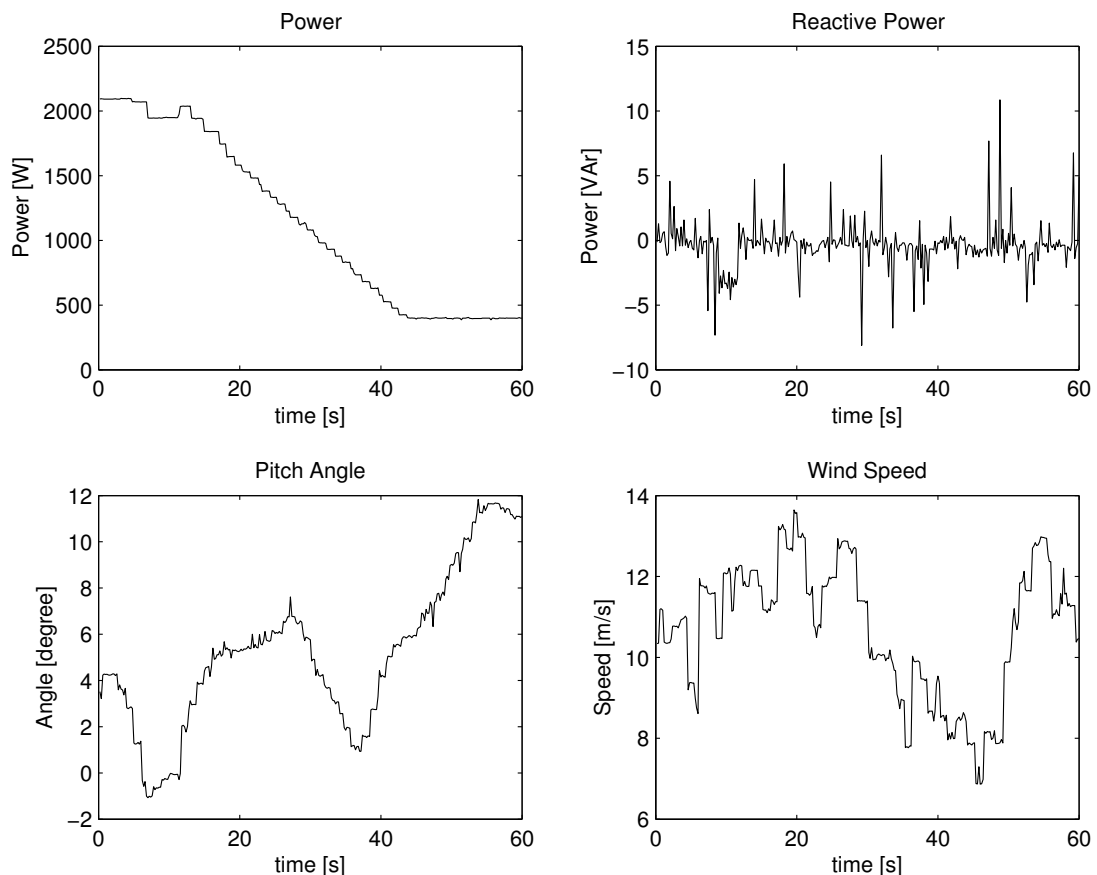


Figure 36: SCADA data for  $P_{ref}=400kW$



In Figure 36 the SCADA data can be seen. The “Power” figure data shows the power output from the wind power turbine. It can clearly be seen that the power is decreasing to 400kW as it is supposed to for the curtailment case  $P_{ref}=400kW$ . A DFIG can compensate for the reactive power needed to magnetize the generator and for some reactive power in the grid as discussed in Chapter (3.2). The reactive power production is shown in the “Reactive Power” figure. In the “Wind Speed” and “Pitch Angle” figures the wind speed is shown and how the power turbine is changing the pitch angle of the blades to compensate for wind variation and different run scenarios. In Figure 37 and Figure 38 the stator and rotor voltages and current for phase “a” is shown. In addition the rotor speed is shown in Figure 38. The rotor speed is the analogue speed calculated in powerLab discussed in Chapter (5.2).

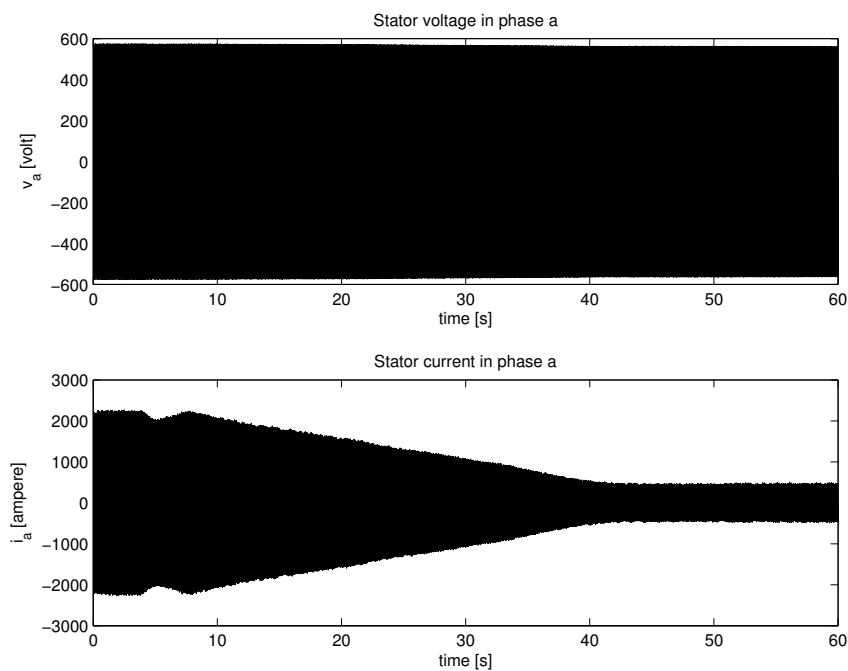


Figure 37: Voltage and current in stator phase “a” for  $P_{ref}=400kW$

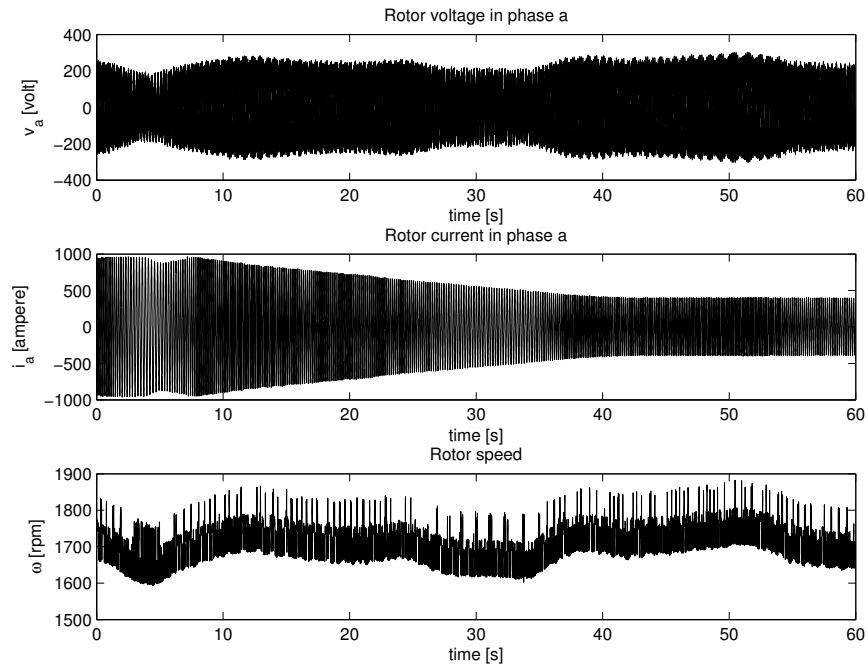


Figure 38: Voltage and current in rotor phase “a” and rotor speed for  $P_{ref}=400kW$

## 6.2 Simulations

Because of corrupted data in the measurements discussed in Chapter (5.1.4) the only run scenarios available for simulation is the curtailment run scenarios with power reference 160 kW and 400 kW and the star/ $\Delta$  switch.

### 6.2.1 Verifying the model

To verify the calculated torque in the dynamic model the torque can be compared with the stationary torque calculated with

$$T = \frac{P}{\omega_m} \tag{51}$$

This is done in Figure 39. The torque in Equation (51) does not take dynamic changes in the speed and rotor dynamics into consideration. The losses and magnetising power is not included in the stationary torque. But it gives a good idea about the size and characteristics of the torque.

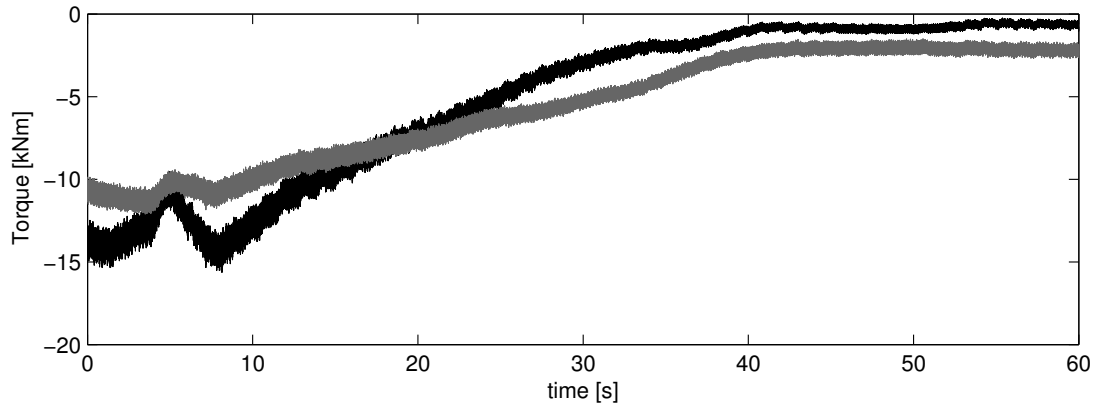


**Figure 39: The dynamic torque calculated in the model (black) and the stationary torque according to Equation (51) (grey).**

In Chapter (5.1.3) the mechanical measurements done are described. Another way to verify the model is to compare the calculated torque with the mechanical torque measured on the high speed shaft. Discussed in Chapter (5.1.4) there are limitations in both the mechanical and electrical measurements, but comparing the two graphs gives a good hint if the calculated torque is in the correct range and got the right characteristics. In Figure 40 the two graphs can be seen for the curtailment run scenario with the power reference set to 400kW for the turbine.

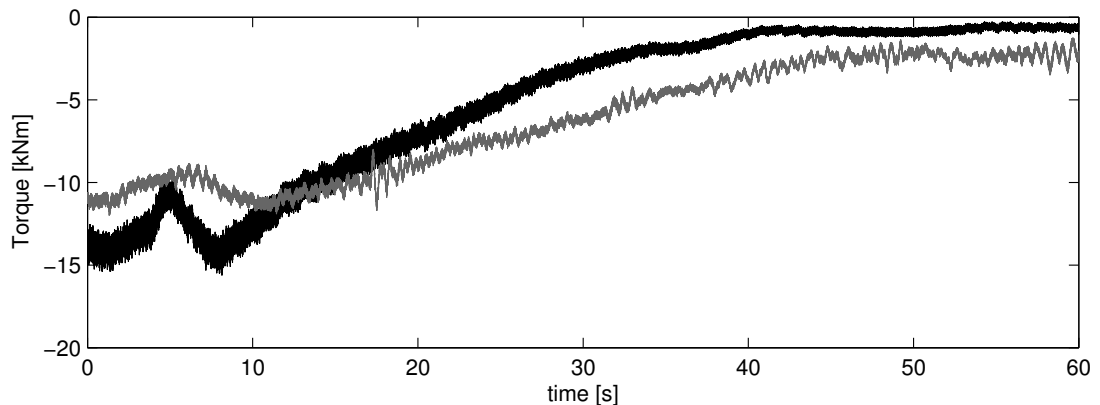


**Figure 40: The dynamic torque calculated in the model (black) and the torque measured (grey)**

## 6.2.2 Uncertainties

In the model there are a number of uncertainties, these are discussed in this chapter.

It can be seen in Chapter (5.4.3) how very small errors in the rotor angle can give rise to simulation error. There are a number of factors that affect the rotor angle and gives uncertainties in the model. The pulse train signal generated by the black and white tape used to calculate the rotor angle is noisy. This signal is therefore filtered and that affect the characteristics of the rotor angle to some extent. There is nor any documentation about the measurement equipment that makes it hard to determine the accuracy of the measured rotor angle.

The initial angle is iterated ocular between two graphs and is discussed in Chapter (5.4.3). There is a certain amount of dynamic in the system. It can not be concluded that the rotor current changes sign at the exact instant the speed passes the synchronous speed, meaning that some dynamics in the induction generator can be unintentionally excluded. If the physical orientations of the coils in the rotor are known it is possible to climb up in the wind turbine and measure the initial angle because the black and white tape is not removed. A large amount of the rotor angle measurement is corrupted so if it is decided to redo the measurements the initial angle for those measurements should be found out.

This Master Thesis is a public document. Due to company disclosure the inductances and inertia constants for the wind power turbine on which the measurements have been done are not used. Instead the constants used are form a public report [20] examine a wind power turbine in the same size. For the inductances, the stator and rotor inductances are relatively small comparing to the magnetising inductance and do not have a great impact on the simulated torque. The magnetising inductance affects the magnitude of the output torque and can do so rather much. Changes in the size of milli Henry can affect the magnitude up to ten times its value. The parameter affects the magnitude of the curve and is important but can be adjusted after the mechanical curve if a rough initial parameter is known. The parameters are only a problem in an open report where the exact constants are not known. The inertia constant only gives high affect to the torque when the speed variations are big. The wind power turbine aims to have an optimal constant speed slightly above the synchronous speed. Therefore the rotor acceleration is seldom over  $5 \text{ m/s}^2$  and do not affect the output in any lager extent and when it does it is during a limited time period

The equations used to describe the mathematical model of the induction generator are from the public report [7]. This report is for a general DFIG and not the specific equations for the test turbine used, this also because of company disclosure. Therefore the test turbine can have dynamics and characteristics not considered in the model.

### 6.2.3 Curtailment run scenario with power reference 160 kW

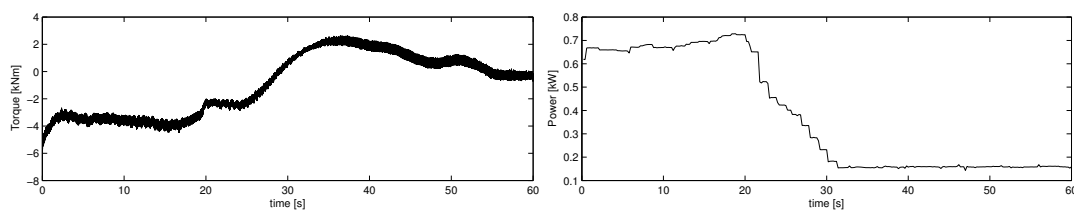


**Figure 41: Dynamic torque calculated in the model (left) and output power according to SCADA-data (right)**

In Figure 41 the curtailment run scenario for the power reference 160 kW can be seen. The right figure shows the SCADA-data there it can be seen how the output power from the turbine is ramped down to the reference level of 160kW. In the right figure the simulated torque is shown. In this figure the simulated mechanical torque becomes negative during the reference change. The long duration of the sign change indicate that it is the mechanical time constant for the turbine that does not correspond with the general model used in this thesis. When the power is ramped down the drive train is accelerated and energy is fed into the system. This could affect the current in the model. The time the simulated torque is negative could be the time it takes for the model to discharge the excess energy mis-balance in the drive train and come back to the proper torque.

6.2.4 Star/ $\Delta$  switch

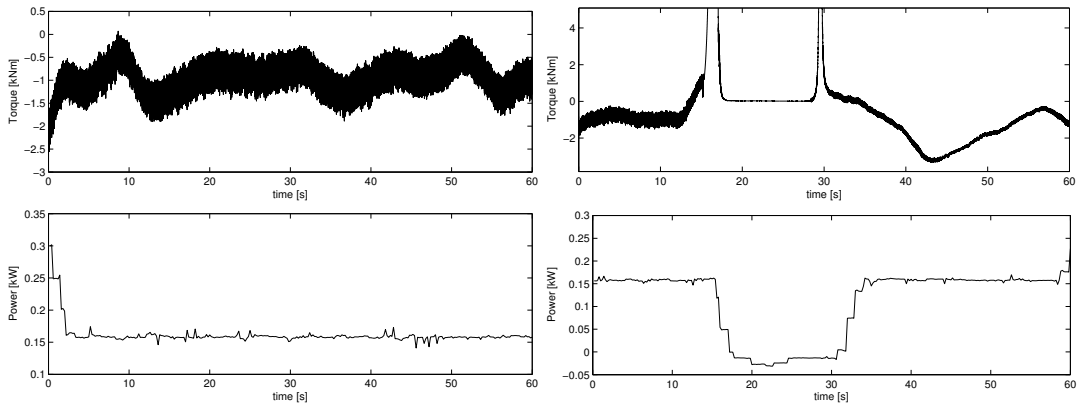


**Figure 42:  $\Delta$  -> star switch with the dynamic torque from the model (top) and output power according to SCADA-data (bottom)**

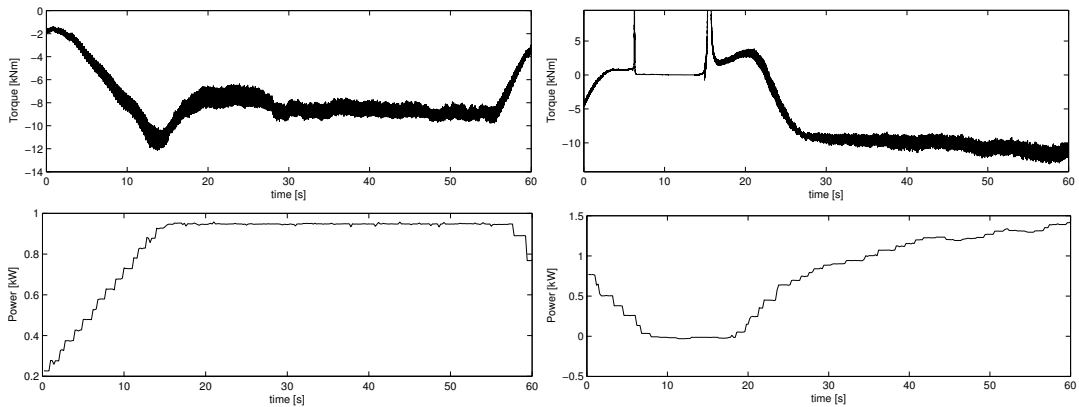


**Figure 43: Star ->  $\Delta$  switch with the dynamic torque from the model (top) and output power according to SCADA-data (bottom)**

In Figure 43 the physical connections of the conductors to the generator is switched from  $\Delta$  connection to star connection. In the top pictures the simulated dynamic torques is shown and in the bottom the power output from the turbine according to the SCADA- data is shown. In the first picture the power reference is set to 160 kW. In the second picture the production has been less than 250 kW long enough and the power is ramped down to zero and the switch from  $\Delta$  connection to star connection is done. The spikes seen in the pictures are from division with zero in the model. In Figure 42 the power is ramped up again to normal production. In star connection the maximum allowed power production power is 950 kW. The wind situation allows higher power production than 950 kW therefore the power is ramped down to zero and the switch from star to  $\Delta$  connection is done. The spikes in the bottom torque picture are also because of division with zero in the model.

## 7 Conclusion

In this “Master Thesis” a big amount of measured data has been handled. A method to convert the measured data, import it in the preferred software and save it together with the SCADA data has been developed. Scripts are developed to calculate the angles for both the rotor and the magnetic flux in the stator. The data has successfully been imported into MATLABs workspace.

To study the measurements for the different run scenarios gives a good picture of how a double fed induction generator in a wind power turbine works and acts in different situations. For example it is concluded in Chapter (5.4.2) that symmetrical modulation was applied. Isolating the different run scenarios and a brief analyse of them did not show any unexpected transient or behaviour.

In this Thesis a mathematical model that calculates the mechanical torque based on the electrical measurements have been derived. In Figure 39 the measured torque is compared with the dynamic calculated torque. It can be seen in the simulations for the different run scenarios that the dynamic calculated torque roughly have the same characteristics. But there is a difference in magnitude. From this it is concluded that the mathematical model can be set up for the measurements and a general model for a double fed induction generator is model Master Thesis.

The gearbox reliability problem is a complex question that the wind power industry all over the world is struggling to solve. It is therefore safe to assume that a certain quality of the data and analyse is required to be able to earn new knowledge about the breakdowns. To reach a high quality in the model this thesis suggests that especially the rotor and stator angle needs to be derived with a more robust method. The mathematical model also must take the test turbines characteristics and dynamics in consideration.

A retake of the measurements with the improvements suggested in this Thesis could lead to an sufficient analyse especially if the accuracy of angle measurement could be verified. A analyse that would reveal information if transients are transmitted from the electrical system and in that case how the different run scenarios characteristics are transmitted from the electrical system to the mechanical drive train. Comparing the simulated mechanical torque with the measured torque would make it possible to see if the torques differ in some scenarios. Differences that could give rise to high forces on shafts and bearings and in the long run could lead to gearbox breakdown. It could also reveal information if transient on the power grid and/or different control strategies for the converter could affect the gearbox.

## 8 Future work

An extension to the Master Thesis is to do a more detailed mathematical analysis about the uncertainties in the dynamic model and how much they affect the output.

To be able to do any more sufficient comparison between the mechanical and electrical torque and increase the knowledge, the mechanical and electrical measurements need to be redone. The measurements need to be done at the same time with the possibility to synchronize the two systems.

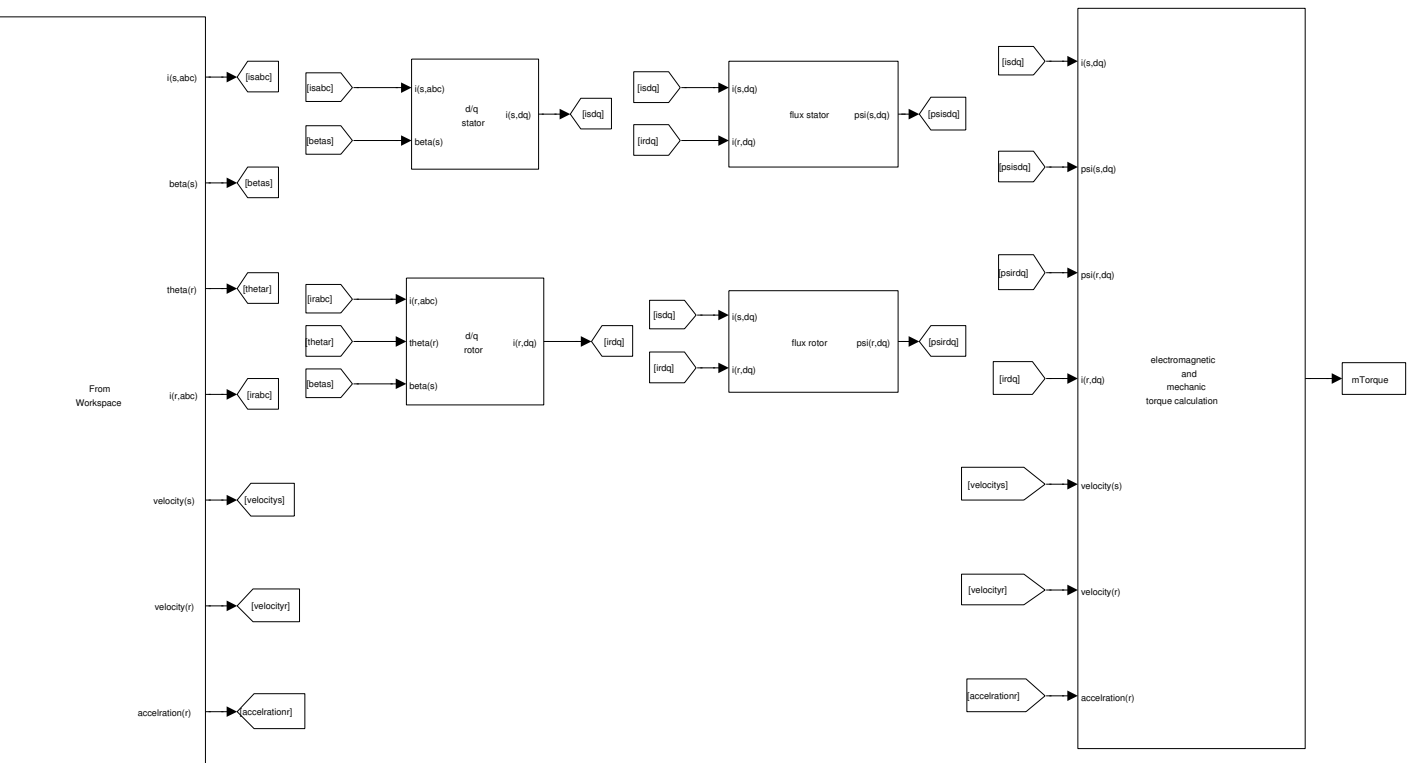
To decrease the uncertainties in the model a more sufficient way to measure the angle and the initial angle would need to be used or developed.

If the measurements is to be redone and the model could be verified more in detailed than in this thesis it would be very interesting to run the different scenarios through the model, analyze the output and compare it to the mechanical measurements. Study differences in torques and accelerations between the simulated and measured torque and investigate if there is any differences and how they affect the gearbox and bearings.

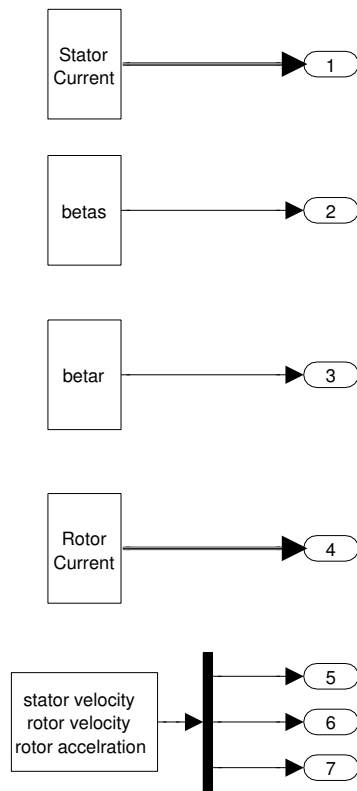
# Appendix A

## Simulation Block Diagrams

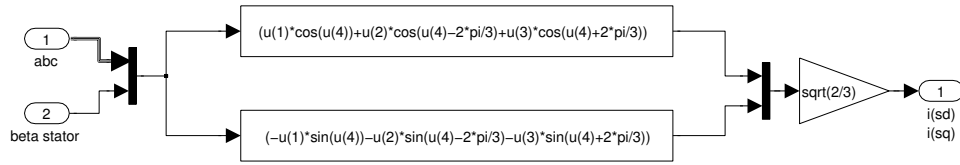




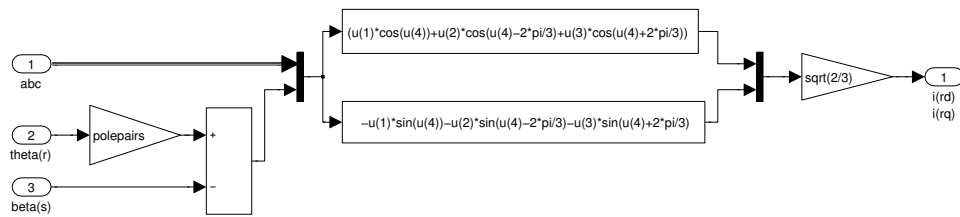
Model of Double Fed Induction Generator



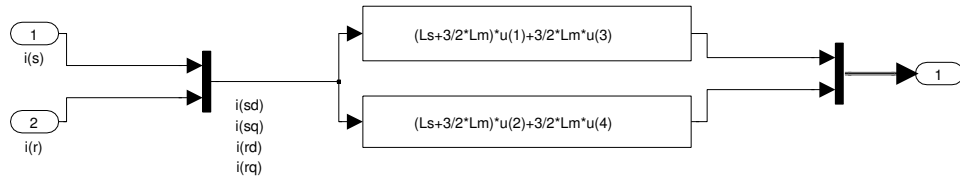
From Workspace



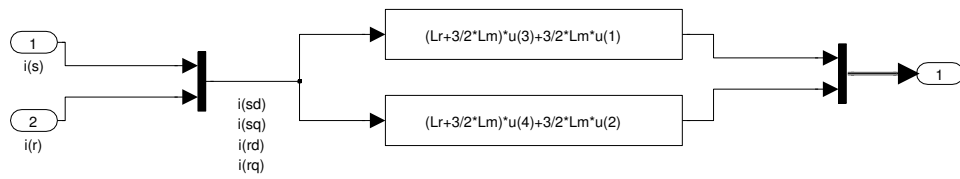
d/q transformation stator



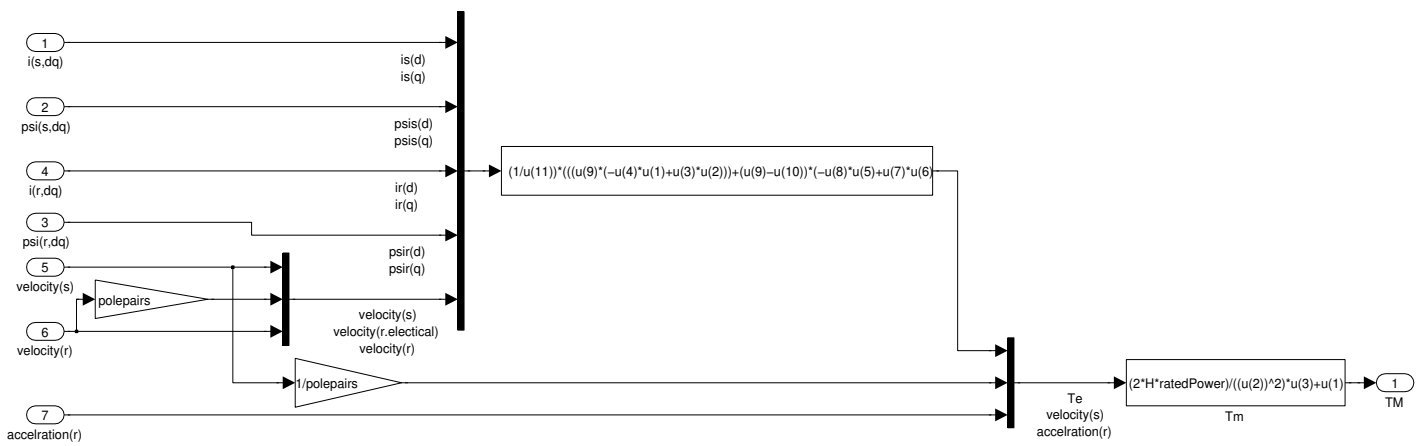
d/q transformation rotor



Stator flux



Rotor flux



Electromagnetic and mechanical torque calculation

# Appendix B

## Simulation File

```
close all
clc
clear all

[FileName,PathName] = uigetfile({'*.mat'}, 'Select a MAT
file(s)', 'MultiSelect', 'on');

if char(FileName(1,1)) == '2'
    l=1;
else
    l=size(FileName,2);
    FileName=sort(FileName);
end

r=1;

while r<=l
    %% load files
    if l==1
        Data_Path=fullfile(PathName,char(FileName));
        PathNameRotorAngle=[PathName '\\' 'Rotor_Angle' '\\'
'Rotor_Angle_' FileName];
        PathNameTurbineAngle=[PathName '\\' 'Turbine_Angle' '\\'
'Turbine_Angle_' FileName];
        FileN=FileName;
    else
        Data_Path=fullfile(PathName,char(FileName(:,r)));
        PathNameRotorAngle=[char(PathName) '\\' 'Rotor_Angle' '\\'
'Rotor_Angle_' char(FileName(:,r))];
        PathNameTurbineAngle=[char(PathName) '\\' 'Turbine_Angle'
'\ ' 'Turbine_Angle_' char(FileName(:,r))];
        FileN=FileName(:,r);
    end

    load(Data_Path, 'Turbine', 'Rotor', 'AuxInfo');
    %% set downsamplesize & polepairs
    decimatesize=10;

    polepairs=2;
    %% downsample Rotor I

    RotorI1=downsample(Rotor.I1,decimatesize);

    RotorI2=downsample(Rotor.I2,decimatesize);

    RotorI3=downsample(Rotor.I3,decimatesize);
    %% downsample Rotor U

    RotorU1=downsample(Rotor.U1,decimatesize);

    RotorU2=downsample(Rotor.U2,decimatesize);

    RotorU3=downsample(Rotor.U3,decimatesize);
```

```

%% downsample Turbine I

TurbineI1=downsample(Turbine.I1,decimatesize);

TurbineI2=downsample(Turbine.I2,decimatesize);

TurbineI3=downsample(Turbine.I3,decimatesize);
%% downsample Turbine U

TurbineU1=downsample(Turbine.U1,decimatesize);

TurbineU2=downsample(Turbine.U2,decimatesize);

TurbineU3=downsample(Turbine.U3,decimatesize);
%% downsample & load Angles

load(PathNameRotorAngle);
load(PatheNameTurbineAngle);

AngleT=downsample(turbine_angle,decimatesize);

AngleR=downsample((rotor_angle),decimatesize);

%% downsample Time

Timedec=downsample(Rotor.Time,decimatesize);

%% calculate Power

Prdec=(RotorU1.*RotorI1+RotorU2.*RotorI2+RotorU3.*RotorI3);

Psdec=(TurbineU1.*TurbineI1+TurbineU2.*TurbineI2+TurbineU3.*TurbineI
3);
Ptdec=Prdec+Psdec;
Time=Rotor.Time;

%% Angle filter

[b,a]=butter(1,.0001);

yinit=-2*pi*50; %init for filter
xinit=AngleT(2)-(AngleT(2)-AngleT(1));
zi=b(2)*xinit-a(2)*yinit;

AngleT_dot=diff(AngleT)./diff(Timedec);

AngleTfilter_dot=filter(b,a,AngleT_dot,zi);

AngleTfilter_dot=[0;AngleTfilter_dot];

yinit=-350/2;
xinit=AngleR(2)-(AngleR(2)-2*AngleR(1));

```



```
zi=b(2)*xinit-a(2)*yinit;

AngleM_dot=diff(-AngleR)./diff(Timedec);

AngleMfiltfilt_dot=filtfilt(b,a,AngleM_dot);

AngleMfilter_dot=filter(b,a,AngleM_dot);

AngleM_dotdot=diff(AngleMfiltfilt_dot)./diff(Timedec(2:end));

AngleMfilter_dotdot=filtfilt(b,a,AngleM_dotdot);

AngleMfilter_dot=[-25*2*pi;AngleMfilter_dot];
AngleMfilter_dotdot=[0;0;AngleMfilter_dotdot];
AngleM_dotdot=[0;0;AngleM_dotdot];
AngleM_dot=[-25*2*pi;AngleM_dot];
AngleT_dot=[-50*2*pi;AngleT_dot];
AngleMfiltfilt_dot=[-25*2*pi;AngleMfiltfilt_dot];

%%

clear Data_Path GPS Speed A...
    PathNameRotorAngle PatheNameTurbineAngle i samplesize
decimatesize ...
    orgsize j k turbine_angle Rotor Turbine t rotor_angle Time

%% run Simulation

sim DFIG ;

%% plot

Tmsim=mTorque(2:end);

figure

plot(Timedec,Tmsim./10^3,'black');
xlabel('time [s]');
ylabel('Torque [kNm]');
set(gca,'PlotBoxAspectRatio',[3 1 1],'xlim',[0 60]);

r=r+1;
end
```

## Bibliography

- [1] Runge Kristoffersen, J. Jensen, L. (2009). *Discussion of Preliminary results*. Tjæreborg. Vattenfall Gerabox Workshop.
- [2] Vattenfall Research and Development AB. Hansen, A. (red.) (2010). *Wind R & D Programme annual report 2009*. Sandvikens tryckeri.
- [3] Wizelius, T. (2007). *Vindkraft i teori och praktik*. Lund. Studentlitteratur.
- [4] Alfredsson, A. Jacobsson, K. Rejminger, A. Sinner, B. Cronqvist, A. (red.) (2008). *Elkraftshandboken: Elmaskiner*. Malmö. Liber AB
- [5] Vestas. (2010). *V80-2MW*. 2010-09-20.  
<http://www.vestas.com/en/media/brochures.aspx>
- [6] Sørensen, P. Hansen, A. Thomsen, K. Buhl, T. Morthorst, P. Nielson, L. (2005). *Operation and control of large wind turbines and wind farms – Final report*. Risø. Risø National Laboratory.
- [7] Elington, K. (2009). *Modelling and control of Double Fed Induction Generators in power systems*. Licente thesis. Stockholm. Royal institute of Technology
- [8] Alaküla, M. Johansson, J. Lindstedt, G. Simonsson, B. (2006). *Grundläggande Elektroteknik*. Lund. KFS AB.
- [9] The University of Nottingham. *3 Phase Induction Motor*. 2010-09-20.  
<http://hermes.eee.nott.ac.uk/teaching/cal/h51elc/elc0026.html>
- [10] Perdana, A. (2003). *Dynamic modeling of Wind Power Generator with Double Fed Induction Generator*. Master Thesis. Stockholm. Department of Electrical Engineering, Royal Institute of Technology.
- [11] Chitti Babu, B. Mohanty, K.B. (2010). *Double-Fed Induction Generator for Variable Speed Wind Energy Conversion Systems – Modeling & Simulation*. International Journal of Computer and Electrical Engineering. Vol. 2. No. 1
- [12] Alaküla, M. Karlsson, P. *Power Electronics: Devices, Converters, Control and Applications*. Lund. Department of International Electrical Engineering and Automation. Lund University
- [13] Vattenfall AB. (2009). *Background for the measurements*. Gearbox Workshop, Tjæreborg 11<sup>th</sup> – 12<sup>th</sup> June.
- [14] Wikipedia, the free encyclopedia. *Fatigue (material)*. 2010-10-26.  
[http://en.wikipedia.org/wiki/Fatigue\\_\(material\)](http://en.wikipedia.org/wiki/Fatigue_(material))
- [15] Runge Kristoffersen, J. (2010). *Vattenfall Wind Power Academy: Introduction to Wind Turbine Technology*. Råckstad. Vattenfall AB.

- [16] Runge Kristoffersen, J. (2009). *Data Overview – Gearbox Measurements in Tjæreborg*. Projekt No. 138.02.03.03. Vattenfall R&D.
- [17] Yagi, S. (2004). *Bearings for Wind Turbine*. NTN Technical Review No. 71
- [18] National Instrument, *Reading TDM/TDMS Files with The MathWorks, Inc. MATLAB® Software*, 2010-06-01, <http://zone.ni.com/devzone/cda/epd/p/id/5957>
- [19] Carlsson, A. (1998). *The back to back converter : control and design*.Lund. Department of Industrial Electrical Engineering and Automation. Lund Institute of Technology.
- [20] Anaya-Lara, O. Arulampalam, A. Bathurst, G. Hughes, F.M. Jenkins, N. (2005). *Transient analysis of DFIG wind turbines in multi-machine networks*. 18<sup>th</sup> International Conference on Electricity Distribution. Turin, 6-9 June 2005.